Electro-catalytic oxidation of hydroxide ion by Co_3O_4 and Co_3O_4@SiO_2 nanoparticles both at particle ensembles and single particle level

Ruo-Chen Xie,[a] Maria Volokhova,[b] Aleksei Boldin,[b] Dr. Liis Seinberg,[b] Dr. Masahiko Tsujimoto,[c] Minjun Yang,[a] Dr. Bertold Rasche,[a] Prof. Dr. Richard G. Compton*[a]

[a] *Department of Chemistry, Physical and Theoretical Chemistry Laboratory, University of Oxford, South Parks Road, Oxford OX1 3QZ, UK. E-mail: richard.compton@chem.ox.ac.uk*

[b] *Chemical Physics Laboratory, National Institute of Chemical Physics and Biophysics, Akadeemia tee 23, 12618, Tallinn, Estonia*

[c] *Institute for Integrated Cell-Material Sciences (iCeMS), Kyoto University Institute for Advanced Study (KUIAS), Kyoto University, Yoshida Ushinomiya-cho, Sakyo-ku, Kyoto 606-8501, Japan*

Abstract

We report that the Co_3O_4 nanoparticle-mediated electrochemical oxidation under alkaline conditions of hydroxide ion on a glassy carbon macroelectrode leads to hydrogen peroxide as the initial oxidation product of electron transfer. The latter is inferred to subsequently partially decompose to dioxygen by catalytic chemical reaction at the nanoparticles. At the single particle level, electrochemical particle-electrode impacts point out the rate-determining step and the limiting kinetics of the reaction. Further, particles with core-shell structure of a Co_3O_4 core and SiO_2 shell are synthesised, and their electrochemical behaviour is studied and compared with bare Co_3O_4 nanoparticles, suggesting the very likely broken or highly porous state of the silica shell, which is not otherwise easily distinguished, for example by electron microscopy.

1. Introduction

Co_3O_4 particles are important electrocatalysts for many reactions in the field of sustainable energy such as the reactions for overall water splitting – hydrogen evolution reaction (HER) and oxygen evolution reaction (OER),[1] for Cl_2 production,[2] and for the electro-oxidation of methanol[3] and glucose in organic fuel cells.[4] As nanoparticles (NPs), they possess large specific surface areas sometimes with an engineered abundance of surface oxygen vacancies,[5] leading to high catalytic activity, whilst the intrinsic origin of the latter is considered to be the valencies of the cobalt cations,[6] which in the case of OER catalysis contributes to the formation of strong surface intermediate-bond of Co-OH in the rate determining step.[7] Co_3O_4 NPs have also been considered to be chemically stable in strongly alkaline conditions,[8] and of practical interest due to the relatively low cost and higher abundance.[9] In particular, the NPs have been recently demonstrated to show an excellent electro-catalytic activity towards OER[5, 10] *via* equation 1:

$$4\ OH^- \rightarrow O_2 + 4\ e^- + 2\ H_2O \qquad (1)$$

which is comparable to or even superior than the noble-metal based materials (e.g. Pt, Ir).[5a] The basis of this comparison is the overpotential at a given current density relative to the electrochemical potential of the OH^-/O_2 couple at thermodynamic equilibrium, and/or the turnover frequency of surface Co cations, for which the faradaic current at a certain potential is measured, both assuming a four-electron transfer process generating dioxygen. To this end, mass spectrometry has been applied to confirm the formation of dioxygen, with isotope (^{18}O) labelling used to show its origin as being from the solution phase,[11] and fluorescence-based oxygen sensors to quantify the faradaic yield of O_2 as nearly 100%.[10d, 10f, 12] The ultimate formation of dioxygen is clear; however, the mechanism by which it is formed remains open and is the focus of the present study. The work focuses on using a glassy carbon electrode as a catalyst support and the analysis of the whole range of potential sweeps, both cathodic and anodic, in contrast to previous studies.[5, 10c, 13] In particular, we consider the possibility that rather than a direct 4 electron process taking place, a mixed electron

transfer/chemical disproportionation mechanism occurs via equations 2&3 as has recently been suggested for oxygen reduction on iron (III) oxide[14] or silver NPs[15]:

$$OH^- \xrightarrow[e^-]{Co_3O_4(s)} \bullet OH \longrightarrow \tfrac{1}{2}\, H_2O_2 \qquad (2)$$

$$H_2O_2 \xrightarrow{Co_3O_4(s)} \tfrac{1}{2}\, O_2 + H_2O \qquad (3)$$

in which the catalytic cycling of O_2 leads to the four electron product, H_2O, although the electron transfers lead only as far as H_2O_2, the two electron product.

Conventionally, drop-cast experiments are performed for the electrochemical studies of solid particles due to the simplicity and ease of operation. However, the surface agglomeration of the drop-casted nanoparticles on the electrode surface has been demonstrated even in the cases of low particle surface coverages,[16] diminishing the catalytic performance of the NP catalysts.[17] Moreover, the diffusion layer overlap of those particles tends to mask their true catalytic activity[18] and often occurs especially when with a high nanoparticle loading on the electrode surface. Over the last two decades, an emerging technique of particle-electrode impacts, or 'nano-impacts', has been demonstrated to provide insights at the single particle level for many electro-catalysis processes including hydrogen oxidation on Pt NPs[19] and Pd NPs[20], methanol oxidation on Pd NPs,[21] oxygen reduction and hydrogen peroxide reduction on single enzymes.[22] The area of catalytic impacts has been recently reviewed.[23] In a typical catalytic nano-impact experiment, the solid particles are well dispersed in solutions containing appropriate electrolyte, and by virtue of their Brownian motion randomly move and eventually may impact on the electrode surface. The impact is likely to result in a short residence of the NPs at the electrode surface held at suitable potentials, which meanwhile mediates the reactions of redox molecules present in solution phases. Consequently, the impact signals with shapes of 'spikes' or 'steps', depending on the particle residence times, may be recorded in the current-time measurements and, in particular, the analysis of the signal current may be able to provide information

regarding the catalytic activity of the *individual* impacting single particles. On this basis, to study the kinetic aspects of Co_3O_4 NPs mediating the OH^- oxidation, single particle electrochemistry will be attempted in addition to the conventional study of the drop-cast particle ensembles. Further, we also investigate the electrochemistry of core-shell Co_3O_4@SiO_2 NPs and compare them with Co_3O_4 NPs, drawing on the successful electrochemical studies of identifying and quantifying broken shells of metal/metal oxide core-shell NPs[24] using drop-cast experiments, and characterising single core-shell Au@Ag using the nano-impact technique.[25]

2. Results and discussion

We first (Section 2.1) characterise the size and chemical composition of cobalt (II) dicobalt (III) oxide (Co_3O_4) particles using Scanning Electron Microscope (SEM) and Energy Dispersive Spectroscopy (EDS). Second, (Section 2.2) we examine the cyclic voltammetric responses (CV) of the Co_3O_4 NPs. Then, (Section 2.3) the voltammetry of Co_3O_4-mediated OH^- oxidation on glassy carbon (GC) electrodes modified with drop-cast Co_3O_4 NP ensembles are studied to evidence their catalytic activity towards this oxidative process. (Section 2.4) The reaction mechanism is discussed with aid of UV spectroscopy. Third, (Section 2.5) we perform nano-impact experiments by making fixed potential, current-time measurements ('chronoamperometry') at a clean glassy carbon micro-disc electrode inserted in a Co_3O_4 nanoparticle suspension, where these particles are on the average spatially well separated with centre to centre distances of *ca.* 1 µm. By virtue of Brownian motion, these particles may stochastically collide with the microelectrode surface held at suitable oxidising potentials. Random current steps were detected in the chronoamperograms, evidencing the catalytic oxidation of hydroxide ions on the *individual* impacting Co_3O_4 NPs for the timescale of their residencies at, or very close to, the electrode surface. Insights into this catalytic process, at the single particle level, are subsequently given. In the Sections 2.6-2.9, similar experiments were performed on silica-coated cobalt (II) dicobalt (III) oxide nanoparticles (Co_3O_4@SiO_2 NPs). Last, the results of the two types of NPs are compared and discussed.

2.1. Characterisation of Co_3O_4 nanoparticles

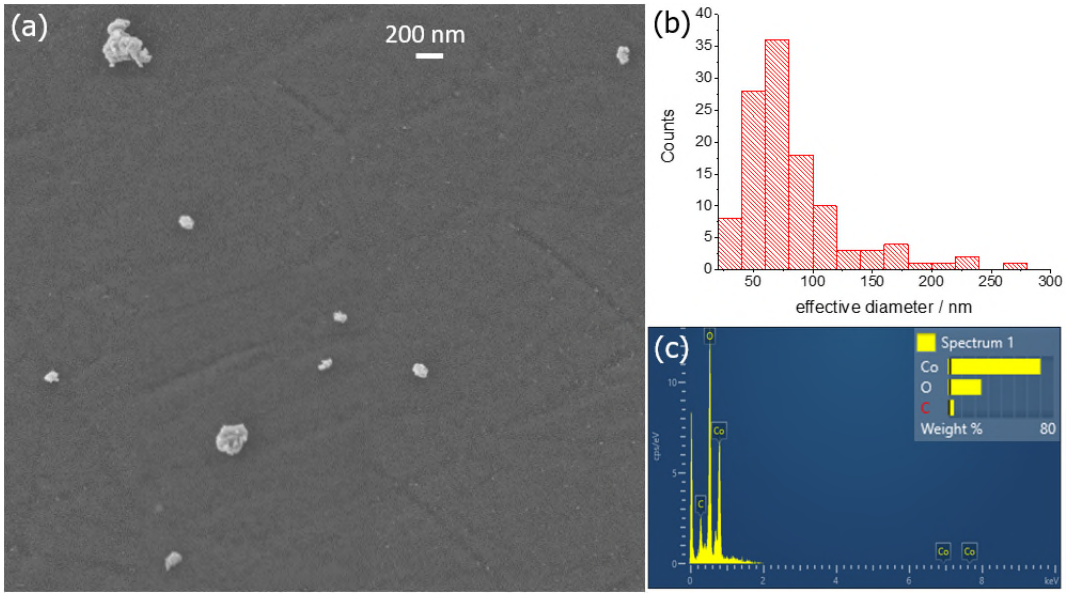

Figure 1. (a) SEM image of Co_3O_4 NPs. (b) diameter distribution of the particles. (c) EDS analysis on of the particles with a Co to O molar ratio of 0.72 ± 0.09 average across three different sites. The presence of carbon detected is consistent with the glassy carbon substrate.

Co_3O_4 NPs were first imaged by SEM and EDS for size and chemical composition analysis, respectively. Figure 1a shows that these NPs are of irregular shapes; for approximate sizing of the particles, the shapes were assumed as perfect spherical and accordingly their peripheries in the 2D images were outlined first as an oval shape. The individual oval areas were measured and then converted to the *effective* diameters of circles of same areas. Subsequently, the average diameter of a total number of 115 Co_3O_4 particles were measured as 75 ± 22 nm (Figure 1b). Meanwhile, Figure 1c illustrates the EDS measured chemical composition of these NPs with weight percentages of cobalt and oxygen elements. The molar ratio of Co to O was calculated as 0.72 ± 0.09, consistent with the expected value of 0.75 for the as-received cobalt (II) dicobalt (III) oxide (Co_3O_4) particles. Note that the existence of Co_2O_3 is thought doubtful.[26] The chemical identity of Co_3O_4 was thus concluded.

2.2. Cyclic voltammetry (CV) of Co_3O_4 NP ensembles

The electrochemical behaviour of Co_3O_4 NPs was first investigated. First, the CV of a bare GC electrode immersed in 0.1 M KCl + 20 mM KOH was performed in the potential range of 0.0 V to 0.40 V as shown in Figure 2. No voltammetric features were seen. Next, 0.6 µg of Co_3O_4 NPs (corresponding to nearly 35% of a monolayer of close packed particles) was drop-cast onto the GC electrode and dried under an N_2 atmosphere. Cyclic voltammetry was then applied to this Co_3O_4 NP-modified electrode immersed in the same electrolyte. Figure 2a shows one small broad oxidation peak at around 0.25 V vs. Ag/AgCl. The inlay presents, after the removal of capacitive current, a better-defined oxidation wave with a peak potential of +0.30 V, with its peak current scaling linearly with the scan rate (Figure 2b), suggesting the oxidation of a surface-bound species. Moreover, the reductive counterpart of the oxidative wave occurred at 0.28 V (peak-to-peak separation ΔE_{pp} is *ca*. 20 mV), implying the quasi-reversible behaviour of this oxidation at 0.3 V. Figure 3 presents a Pourbaix diagram of the predominant cobalt species. The measured mid-point peak potential of the pair (0.29 V) was found to be close to the thermodynamic potential (+0.22 V vs. Ag/AgCl) for the redox couple Co_3O_4/CoOOH, from the data of Gibbs energy of formation of the cobalt oxide species provided in the literatures at 298 K. [27] Therefore, the first peak is attributed to the reaction 4:

$$Co_3O_4 + OH^- + H_2O \rightarrow 3\ CoOOH + e^- \quad (4)$$

Next, the potential region was extended to a more positive value, +0.65 V, and a second sharp oxidation wave with a peak potential of 0.59 V was seen (Figure 2a). The peak current of this oxidative wave was again directly proportional to the applied voltage scan rate (Figure 2b) and a back peak at *ca.* 0.58 V (with ΔE_{pp} = 15 mV) was observed. These suggest the second wave as also being due to a quasi-reversible surface-bound reaction. The mid-point potential of the redox peaks (0.58 V) was found to be very close to the thermodynamic potential for the redox couple CoOOH/CoO_2, +0.56 V vs. Ag/AgCl. Moreover, the oxidation charges measured from the two oxidative waves at 0.3 V and

0.6 V have a ratio of 1 to 3, agreeing with the number ratio of electrons transferred per cobalt atom of the two reactions. Therefore, the second oxidation was attributed to the reaction 5:

$$CoOOH + OH^- \rightarrow CoO_2 + H_2O + e^- \quad (5)$$

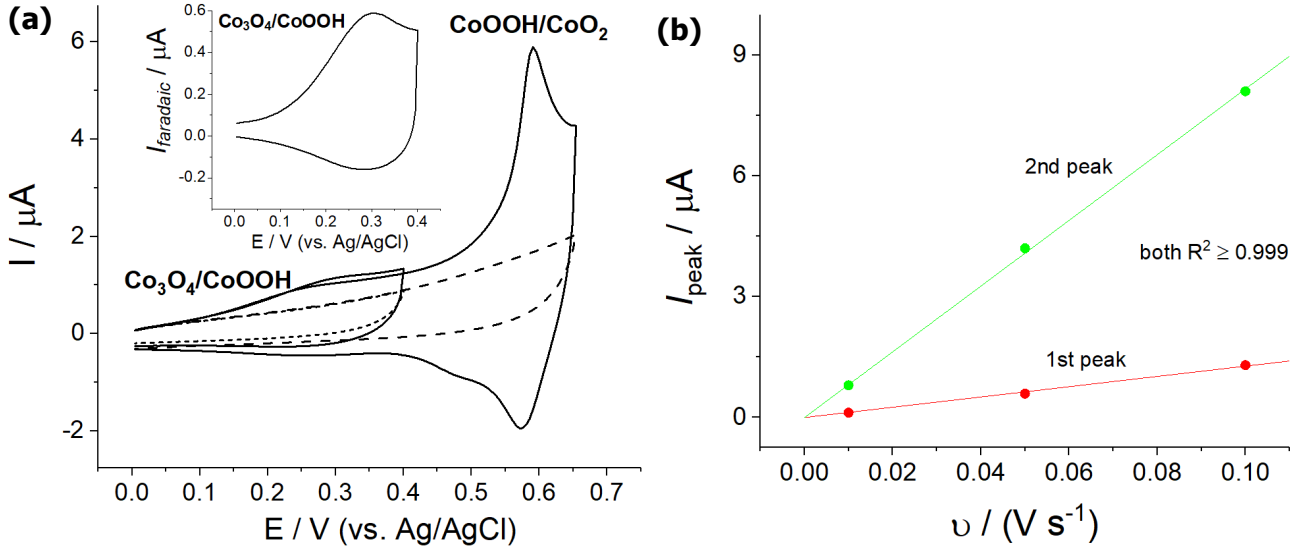

Figure 2. (a) Cyclic voltammomgrams of bare GC electrodes (dashed curves) and the ones modified with Co_3O_4 NPs (solid curves) immersed in 0.1 M KCl + 20 mM KOH solutions in the anodic potential ranges of 0.0 V to 0.40 V and to 0.65 V, respectively. A conversion of the potentials against Ag/AgCl to those against reversible hydrogen electrode (RHE) is provided in SI section 1. Scan rate 50 mV s^{-1}. Inlay: the 'Faradaic current' voltammogram of 0.0 to 0.4 V, obtained from the background current subtraction on the measured drop-cast voltammogram. (b) Plots of peak current of the two oxidation peaks at 0.3 and 0.6 V, respectively, as a function of scan rate.

Nevertheless, we note that the total charge measured from the two oxidative waves was 8.8 ± 2.0 µC, significantly smaller than the expected charge for complete oxidation of drop-cast Co_3O_4 NPs (*ca.* 1 mC) *via* the two-step oxidation to CoO_2, yet comparable to the value of 31 µC estimated for the oxidation of only the NP surfaces assuming a monolayer of the surface of the Co_3O_4 NPs was oxidised (to CoO_2) (see SI section 2a). This suggests the oxidation of the NPs only occurs at the particle

surfaces, implying that possibly the surface oxidation products of Co_3O_4 are non-conductive, and/or the solid state diffusion of the oxidised cobalt species inhibits further reactions of the inner parts.

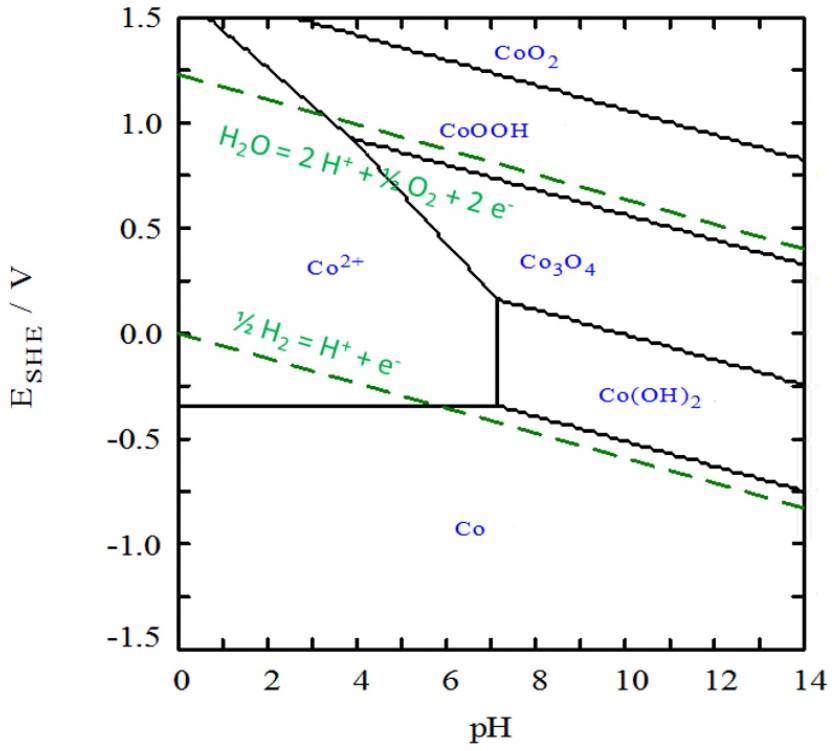

Figure 3. Pourbaix diagram of predominant species calculated for bulk phases of cobalt in aqueous solution at 298 K. The total concentration of Co was fixed at 10 mM. Adapted from Ref. [27a].

2.3. Cyclic voltammetry of hydroxide ion oxidation mediated by Co_3O_4 NPs

To investigate the possible hydroxide ion oxidation, the CVs measured above were further extended to a positive potential of +1.2 V and to a more negative potential region (-1.4 V), as seen from Figure 4. For the dropcast Co_3O_4 NPs, the particle surface coverage was calculated to be *ca.* 35% of a monolayer, assuming the particles were evenly distributed on the electrode surface (See SI section 2b), although in practice, the NPs likely form agglomerates on the electrode surface through the drying process.[16] Consequently, in the anodic region the CV of the Co_3O_4-modified electrode shows, apart from the NP oxidation peaks between 0.1 and 0.6 V, a large oxidative wave peaking at 1.0 V. The peak current of the latter was found to scale linearly with the square root of voltage scan rate as

seen from Figure 5a and to be proportional to the concentration of hydroxide ion in solutions (Figure 5b), with no peak observed in the absence of deliberately added hydroxide ions. These suggest the process is attributed to diffusion-controlled oxidation of OH^-. In the absence of the NPs, no voltammetric features were observed in the extended potential region of 0.65 to 1.20 V, indicating that the oxidative wave at 1.0 V is OH^- oxidation catalysed by Co_3O_4 NPs.

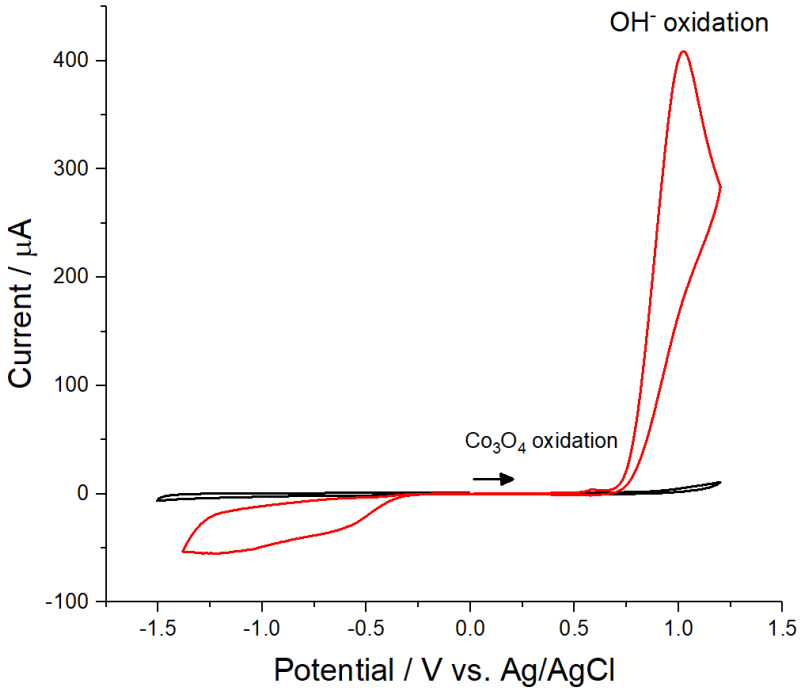

Figure 4. Cyclic voltammomgrams of a bare GC electrode (d = 3.00 mm) and one modified with Co_3O_4 NPs (particle surface coverage of 35%) immersed in 0.1 M KCl + 20 mM KOH solutions. Scan rate 50 mV s^{-1}. The scans start from 0.0 V.

Further upon the study of the OH^- oxidation peak, an average anodic transfer coefficient (β) of 0.47 ± 0.06 was obtained by Tafel analysis (See Figure S1 in the SI section 3) in the region of 20%-30% of the peak current.[28] From the slope of the fitted straight line in Figure 5a, one can derive the number of electron transferred via the Randles-Sevcik equation for 298 K

$$\mathrm{I}_p = 2.99 \times 10^5 \sqrt{n' + \beta_{n'+1}}\, n\, D^{1/2}\, c^* A\, v^{1/2} \qquad (6)$$

where I_p is the peak current, n' the number of electrons transferred before the rate determining step, $\beta_{n'+1}$ the transfer coefficient of the rate determining step, n the total number of electrons transferred, D the diffusion coefficient (4.60×10^{-9} m^2 s^{-1})[29] of OH^-, c^* the bulk concentration of OH^-, A the electrode surface area and v the scan rate. The total number of electrons transferred was thus calculated to be 0.96 ± 0.14, indicating a one-electron-transfer process for the oxidation of hydroxide ion, very probably to H_2O_2 (see the next section).

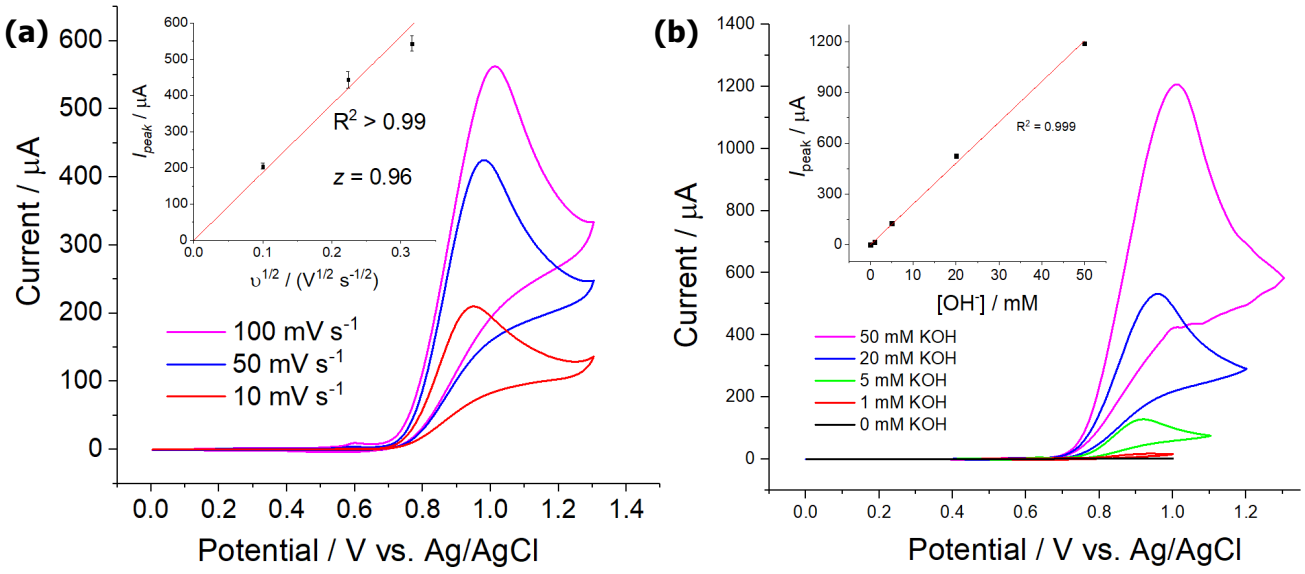

Figure 5. (a) Anodic voltammograms of a Co_3O_4 NP-modified electrode in 0.1 M KCl + 20 mM KOH. Scan rate varies from 10, 50 to 100 mV s^{-1}. Inlay shows the linearity between the peak current and the square root of scan rate. (b) Voltammograms of a Co_3O_4 NP-modified GC electrode (d=3.00 mm, NP surface coverage 35%) in 0.1 M KCl containing varying concentrations of KOH from 0 mM to 50 mM. Scan rate 50 mV s^{-1}. Inlay shows the linearity between the peak current and the hydroxide ion concentration.

2.4. Mechanistic studies of the hydroxide ion oxidation

To further elucidate the mechanism of the hydroxide ion oxidation catalysed by cobalt (II) dicobalt (III) oxide nanoparticles, the negative potential region in Figure 4 was first studied. As seen from

Figure 6a, on the reverse scan to a very negative potential (-1.4 V), a peaked broad reductive wave was seen with a peak potential of -1.2 V, with a small shoulder peak at *ca.* -0.6 V. To study the origin of this reduction current, in an N_2-saturated 0.1 M KCl + 20 mM KOH solution, the CVs of Co_3O_4 NP-modified GC electrode was additionally performed from 0 V to +0.65 V to -1.4 V (red dashed curve) and also directly to -1.4 V (blue curve). Consequently, the broad reductive wave was not found in either of the two cycles, indicating that the reduction was related to the generated species from the OH^- oxidation.

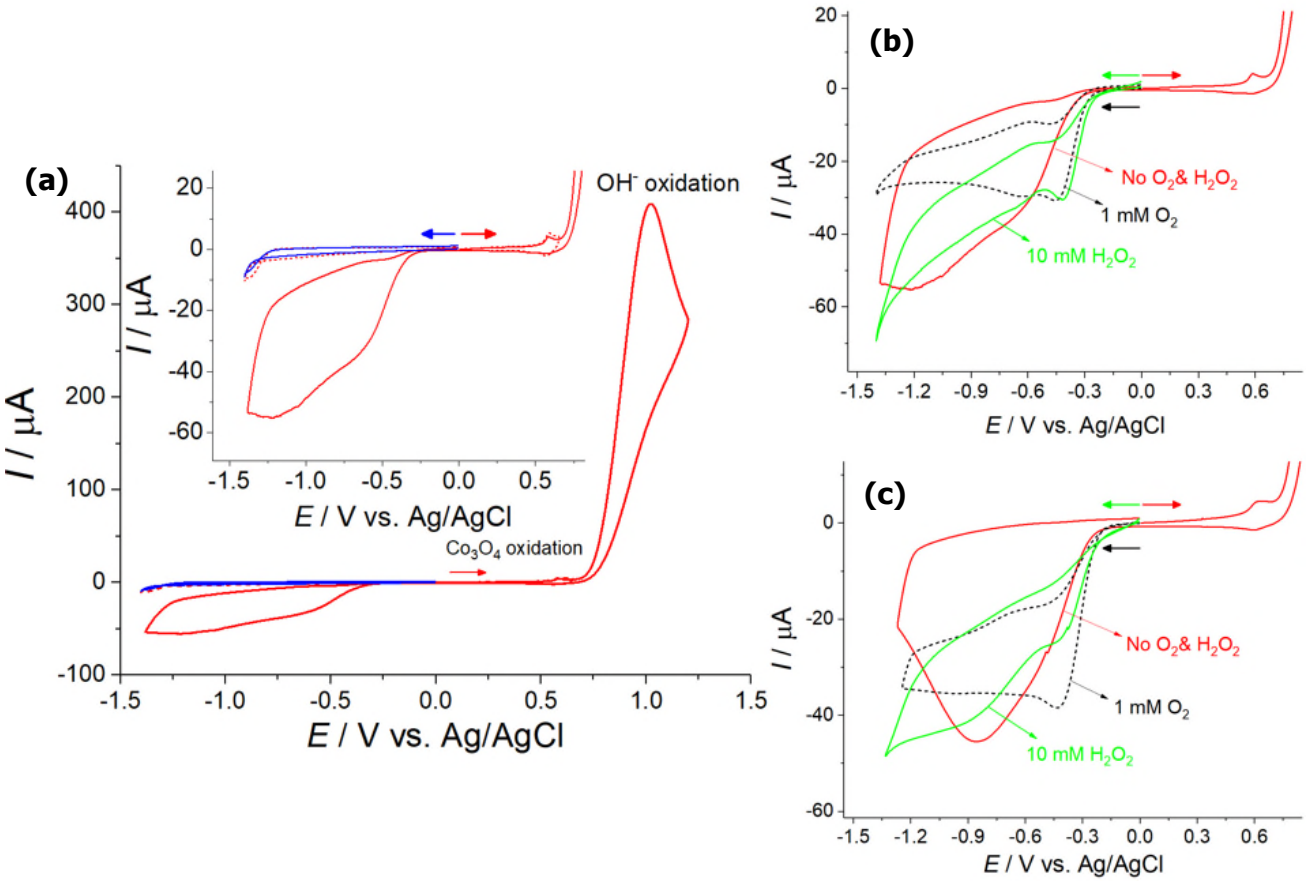

Figure 6. a) Voltammograms of a Co_3O_4 NP-modified electrode in degassed 0.1 M KCl + 20 mM KOH. Inlay shows the enlarged region of the broad reduction wave and the additional two cycles for comparison. Fingerprinting voltammograms of O_2 reduction and H_2O_2 reduction in b) 20 mM KOH and c) 10 mM $Ca(OH)_2$ alkaline solutions.

It is noteworthy that in the anodic region at around +1.0 V, gas bubble formation was visually observed on the GC electrode surface. This was inferred to be possible generation of gaseous O_2. Nevertheless, as the OH^- oxidation process has been shown as a one-electron-transfer process, hydrogen peroxide (H_2O_2) is very likely the immediate, direct electrolysis product, whereas the gaseous oxygen may result from the chemical process of the disproportionation of H_2O_2 under the prevailing conditions, given that H_2O_2 is prone to disproportionating under alkaline conditions encouraged by the formation of HO_2^-,[30] and more importantly Co_3O_4 NPs have been suggested as a heterogeneous catalysts for H_2O_2 decomposition.[1, 31] In order to investigate which of the two (H_2O_2 or O_2) was the predominant final product or their proportions in the product mixture, the broad reductive wave was fingerprinted by recording the CVs of Co_3O_4 NP-modified GC electrodes in the same electrolyte saturated with dissolved oxygen (*ca.* 1 mM) and in the one thoroughly degassed using N_2 but containing 10 mM of hydrogen peroxide, respectively. Figure 6b shows that in the voltammogram of oxygen reduction, two peaks were seen at -0.45 and -0.6 V, respectively, followed by a quasi steady-state current. It is clear that except the minor feature of the small peak at -0.6 V, the overall voltammetric features differed significantly from those of interest, precluding dioxygen as a major, direct oxidation product of the OH^- oxidation.

For hydrogen peroxide reduction (green curve in Figure 6b), the wave shows a peak at -0.45 V, which is almost identical to the peak at -0.45 V found in the oxygen reduction voltammogram and therefore suggests the possible chemical decomposition of H_2O_2 catalysed by Co_3O_4 NPs upon immersion of the electrode; further interestingly, a small peak at -0.6 V is seen followed by an ever increasing reductive current prior to solvent breakdown. The absence of any peak features at potentials more negative than -0.6 V may result from the changed mass transport conditions. Unlike the condition in the hydroxide ion oxidation voltammogram where the electro-generated species was only present locally near the electrode surface, the conditions in the H_2O_2 reduction voltammogram always provide a bulk concentration that can constantly supply peroxide to the electrode surface by diffusion. Nonetheless,

the voltammogram of hydrogen peroxide reduction is broadly consistent in terms of wave shape with the reductive current recorded after OH^- oxidation, suggesting H_2O_2 as the major product from the OH^- oxidation. Moreover, similar but distinct voltammograms for the fingerprinting study were also obtained in alkaline conditions using $Ca(OH)_2$ rather than KOH (Figure 6c). At -0.85 V, A distinct broad reduction peak recorded after OH^- oxidation was observed. In the voltammogram for H_2O_2 reduction, apart from the small peak at *ca.* -0.45 V of probably the same origin as in the case of KOH, a reductive wave at a very similar potential of close to -0.9 V was seen, whilst the oxygen reduction voltammogram stays almost the same to that seen in KOH solutions. The consistency in the peak potentials of *ca.* -0.85 V, together with the observations discussed above, further confirmed that the major product of OH^- oxidation was H_2O_2, *via* the reaction 7:

$$OH^- \xrightarrow{Co_3O_4(s)} \tfrac{1}{2}\, H_2O_2 + e^- \qquad (7)$$

It follows that although the gas bubbles were seen on the electrode surface, the decomposition of electro-generated H_2O_2 to O_2, catalysed by Co_3O_4 NPs, occurred only to a marginal extent as they are subject to slow chemical kinetics relative to the OH^- oxidation and on the timescale of the experiments. This inference was supported by the subsequent UV spectroscopic study of the kinetics of the catalytic decomposition of H_2O_2 as next reported. Experimentally, in absence of Co_3O_4 NPs the UV spectra (Figure 7a) of hydrogen peroxide of varying concentrations from 0 to 10 mM in 20 mM KOH solutions were first obtained. No decline over time in the UV absorbance was observed. Figure 7b shows that the absorbance (at 254 nm) scaled linearly with H_2O_2 concentration, but the spectra are consistent with HO_2^- rather than H_2O_2, reflecting the pK_a of 11.6 for the H_2O_2/HO_2^- equilibrium at 298 K.[32], [33], [34] Next, in the presence of Co_3O_4 NPs, the UV aborbance (Figure 7c) of HO_2^- was found to linearly decrease with time (measured within 3 mins), showing the catalytic activity of the NPs towards the chemical decomposition under the alkaline condition via equations 8&9:

$$H_2O_2 + OH^- \rightleftharpoons H_2O + HO_2^- \qquad (8)$$

$$HO_2^- \xrightarrow{Co_3O_4(s)} \tfrac{1}{2}\, O_2 + OH^- \qquad (9)$$

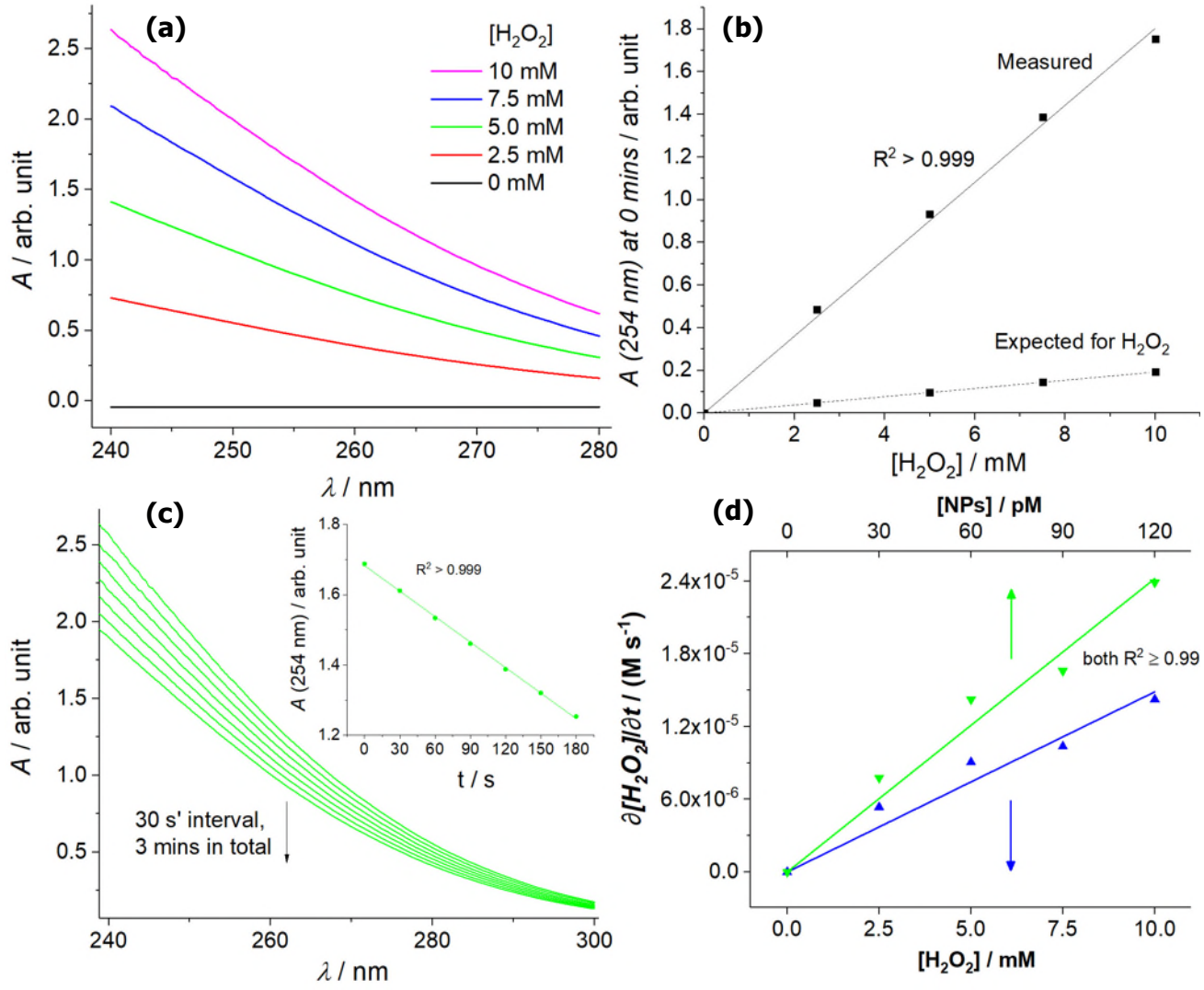

Figure 7. a) UV spectra of 0-10 mM H_2O_2 in 20 mM KOH in absence of Co_3O_4 NPs. b) UV absorbance at 254 nm plotted as a function of H_2O_2 concentration. c) UV spectra of 10 mM H_2O_2 in the presence of 60 pM Co_3O_4 NPs over time. Inlay shows the measured absorbance at 254 nm plotted as a function of time. d) The rate of H_2O_2 decomposition plotted as a function of nanoparticle concentration (green) and of hydrogen peroxide concentration (blue).

From the initial slope of absorbance over time plot, the rate of decomposition was calculated. Subsequently, Figure 7d shows that the decomposition rate scaled linearly with the concentration of Co_3O_4 NPs, suggesting a first order chemical process with respect to the concentration of the NPs. Likewise, the linearity between the decomposition rate and H_2O_2 concentration suggests a first order

chemical process with respect to the peroxide concentration. Therefore, an overall second order kinetics of the peroxide decomposition catalysed by Co_3O_4 NPs was inferred:

$$J = k_0 [NP] [HO_2^-] \quad (10)$$

where J is the reaction flux (M s^{-1}), k_0 the rate constant (M^{-1} s^{-1}), [NP] the particle concentration of Co_3O_4 NPs (M) and $[HO_2^-]$ the bulk concentration of the deprotonated H_2O_2 (M). As such, the k_0 was calculated as 2.7 (± 0.3) × 10^7 M^{-1} s^{-1}. For a direct comparison in the reaction rates of this heterogeneous catalysis process with the electrochemical process of OH^- oxidation, knowing the total NP surface area, the reaction flux J can be converted to an interfacial reaction flux J_i (M m^{-2} s^{-1}) of the peroxide to the NP surfaces by

$$J_i = \frac{J}{[S_p]} \quad (11)$$

where $[S_p] = S_p^o \times [NP]$, $[S_p]$ is the total NP surface area per unit volume (m^2 L^{-1}) and S_p^o is the total NP surface area per mole of Co_3O_4 NPs (m^2 mol^{-1}). Then we have

$$J_i = \frac{k_0 [HO_2^-]}{S_p^o} \quad (12)$$

So that we define an equivalent interfacial rate constant k_i as

$$k_i = \frac{k_0}{S_p^o} \quad (13)$$

Consequently, assuming the diameter of the Co_3O_4 NPs is 75 ± 22 nm as measured from SEM, k_i is determined as 2.5 ± 1.5 × 10^{-4} cm s^{-1}, which is significantly slow as compared to the *limiting* electrochemical rate constant (2.0 ± 1.0 × 10^{-2} cm s^{-1}) for OH^- oxidation measured from the single particle electrochemistry results as will be derived in next section. Hence, the UV spectroscopy results support the conclusion of O_2 as a marginal product due to the rather slow formation kinetics from hydrogen peroxide that was consequently considered as the predominant product of the electro-oxidation of OH^- at Co_3O_4 NP surfaces.

2.5. Single particle electrochemistry of Co_3O_4 NPs

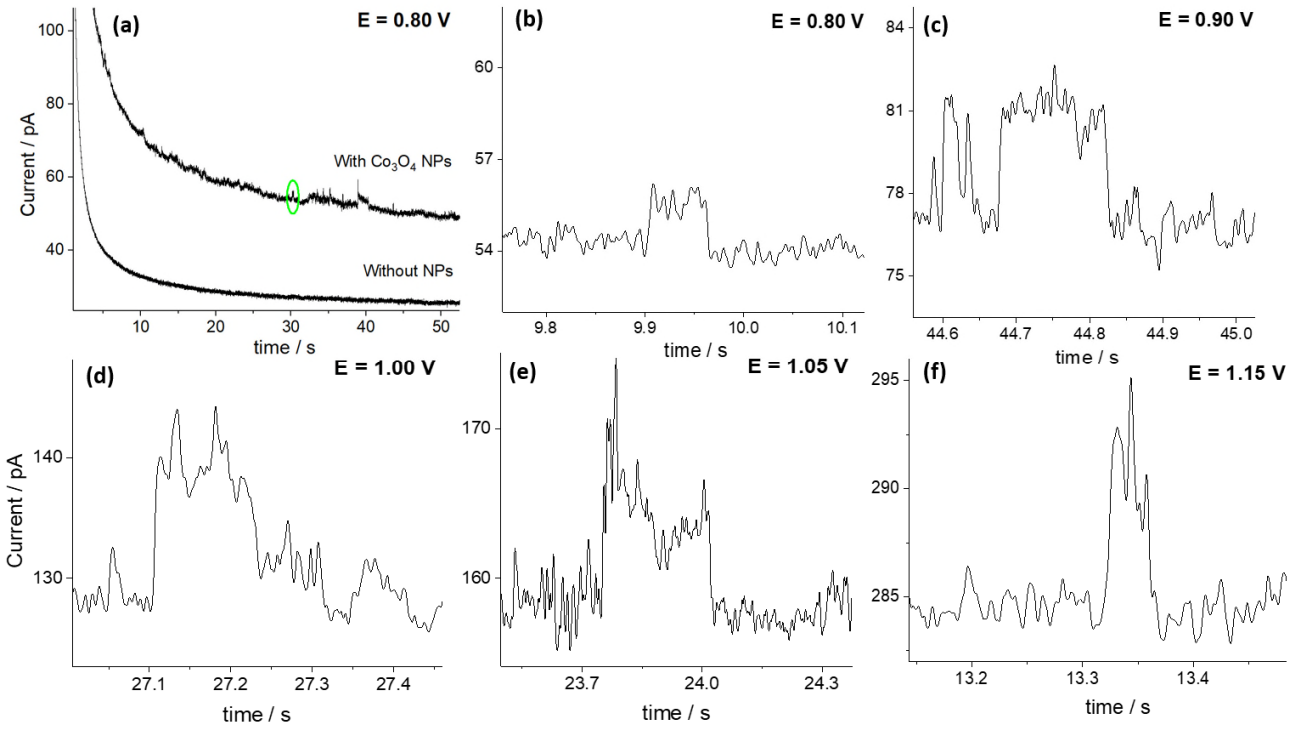

Figure 8. (a) Chronoamperograms of a carbon micro-disc electrode (d=7 μm) immersed in a 20 mM KOH + 0.1 M KCl solution containing 10 mg mL^{-1} Co_3O_4 NPs, held at a potential of 0.80 V vs. Ag/AgCl. Current steps are seen (outlined by the green circle) as enlarged in **(b)**. Examples of representative steps at higher potentials (0.90~1.15 V) are shown in **c-f**. No steps are detected below/at 0.70 V.

Having discovered and studied the hydroxide ion oxidation catalysed by Co_3O_4 NP ensembles, we next conducted nano-impact experiments to probe this electro-catalytic process at the single particle level. Experimentally, a freshly polished carbon micro-disc electrode (d=7 μm) was first dipped in a 20 mM KOH + 0.1 M KCl solution, to which chronoamperometry was recorded at 0.80 V vs. Ag/AgCl for 60 seconds. No features was observed as seen from Fig. 8a. Next, 10 mg mL^{-1} (or 12 nM) Co_3O_4 NPs were added into the solution, where individual suspended particles randomly move by virtue of Brownian motion, although many particles were seen sedimenting out from the suspension. Upon particle collisions with the electrode held at the oxidising potentials (0.8-1.2 V), clear current steps were observed in the chronoamperograms (Fig. 8b-f), evidencing the impacts of the individual Co_3O_4

NPs. Below +0.7 V inclusive, no impact signals regarding the oxidation of Co_3O_4 NPs were detected (See Figure S2 in the SI section 4).

On the average, 50 current steps were obtained at each of these potentials (Figure 9a). The mean impact frequencies as a function of potentials were plotted (Figure 9b), from which over the potential range of 0.80 to 1.15 V the impact frequency was found to stay nearly the same with a mean value of 0.20 ± 0.13 s^{-1}. Each step was assumed to result from the impact events of individual 75 nm diameter NPs and their diffusion coefficient in the aqueous solution was estimated as 6.5 × 10^{-12} m^2 s^{-1} *via* Stokes-Einstein equation,[35] which allows an estimation of the bulk particle concentration to be made using the equation[36]

$$J = 4\,D\,c^{*}\,r \qquad (14)$$

where J is the diffusional flux (or herein the impact frequency) of the NPs towards the electrode surface, D the diffusion coefficient of the NPs in the suspension, c^{*} the bulk concentration of the NPs and r the electro-active radius of the carbon microelectrode. As a result, this frequency suggested a suspended Co_3O_4 particle concentration of 4 ± 3 pM (*ca.* 0.3% of the initial amounts). This is consistent with the experimental observation mentioned above that only a tiny fraction of the particles remained suspended, giving an estimate of an average inter-particle distance of *ca.* 1 μm that indicates those suspended particles were well-separated.

The average step height (current) at +0.8 V were measured as 1.1 ± 0.2 pA, with a step duration of *ca*. 130 ± 40 ms. This duration may be limited by the oxygen bubble formation and collapse (agitation) upon the catalysis process of the impacting particles, or simply result from the diffusional departure of the particles from the interface.[23c] At more positive potentials, increasingly higher steps were measured from 0.80 to 1.00 V with a current plateau at *ca.* 5.7 ± 1.5 pA, as shown in Figure 9a that depicts the average impact step currents as a function of applied potentials in comparison with the

anodic voltammogram of the drop-cast Co_3O_4 nanoparticle ensembles. The threshold potential above which the current steps were found is shown to superpose with that of the catalytic current of hydroxide ion oxidation on the drop-cast Co_3O_4 NPs; and the impact step currents starts to plateau out at 1.00 V, agreeing well with the peak potential of the anodic voltammogram. These observations strongly indicate the catalytic oxidation of OH^- occurring on the individual impacting Co_3O_4 NP surfaces.

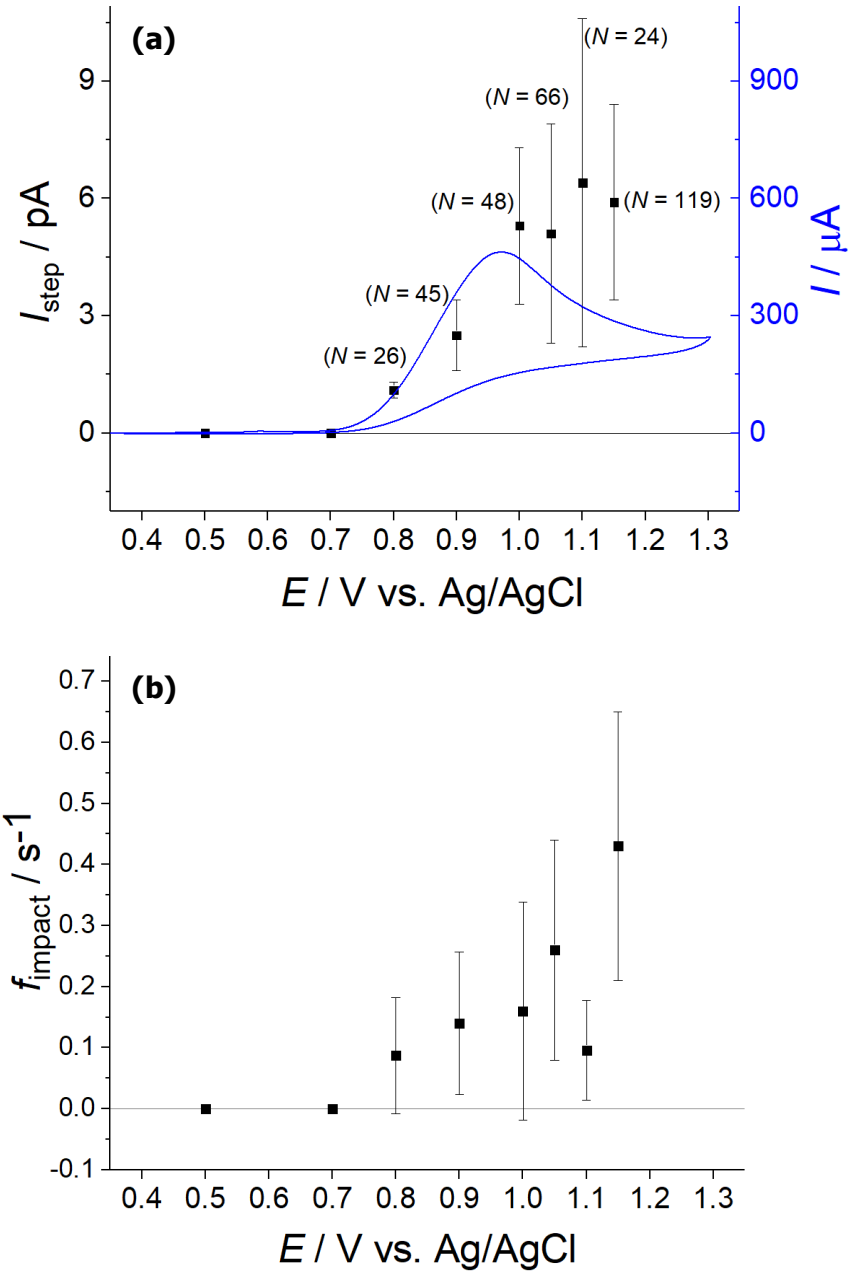

Figure 9. (a) Overlay of the plot (black) of average impact step currents (error bars represent the interdecile range) as a function of applied potentials with the anodic voltammogram (blue) of Co_3O_4 NP ensembles immobilised on a GC electrode. (b) Impact frequency plot as a function of applied potentials.

Further insights regarding the catalysis of OH^- oxidation on *individual* single NP surfaces can then be discussed on the basis of the impact current measured. Given that the catalytic process is a first order catalytic reaction of hydroxide ion (as $I_{peak} \propto [OH^-]$ observed from Figure 5b), the limiting rate constant k_{lim} under the condition was derived from the average step currents I_{step} from 1.00 to 1.15 V using the equation:

$$I_{step} = n\,F\,A\,k_{lim}\,[OH^-] \tag{15}$$

where n is the number of electrons transferred, F is the Faraday constant (96485 C mol^{-1}), A is the catalysing surface area of the impacting NP and $[OH^-]$ the bulk concentration in solutions. As such, the rate constant k_{lim} was found to be $2 \pm 1 \times 10^{-2}$ cm s^{-1}. By contrast, the estimated mass transport coefficient m_T was approximately given by the equation:

$$m_T = \frac{D_{OH^-}}{\delta} \sim \frac{D_{OH^-}}{r_p} \tag{16}$$

where D_{OH^-} is the diffusion coefficient in the electrolyte condition, δ is the diffusion layer thickness of OH^- on the NP surfaces, r_p is the Co_3O_4 nanoparticle radius. As such, the mass transport coefficient was calculated to be *ca.* 10 cm s^{-1}, which is significantly larger than the k_{lim}. This suggests, at single particle level, that the reaction at the individual impacting NP surfaces is a surface reaction rate limited process. However, as seen above for the particle ensembles on a macroelectrode, where a linear regime of mass transport prevails, a diffusion controlled process was observed, consistent with the relatively fast heterogeneous rate constant measured.

2.6. Characterisation of Co_3O_4@SiO_2 NPs

Based on the successful study of hydroxide ion oxidation catalysed by bare Co_3O_4 NPs, our research turned to the novel core-shell NPs with Co_3O_4 cores and SiO_2 shells (Co_3O_4@SiO_2). First, these nanoparticles were synthesised and imaged using TEM. Figure 10a shows the image of a single Co_3O_4@SiO_2 NP. The core-shell structure and their quasi-spherical shapes of both parts were clearly revealed after appropriate adjustments of the image brightness and contrast, allowing the size measurements of the two different compositions. A number of synthesised particles were imaged (Figure 10e) and few particles were found without a core (2 out of 26), giving an average core diameter of 107 ± 27 nm and an overall (core + shell) diameter of 151 ± 45 nm (N = 24).

Next, the chemical composition and structure of the Co_3O_4@SiO_2 NPs were measured by EDS and XRD. As labelled with 'EDS1' and 'EDS2' in Figure 10a, corresponding to the locations of Co_3O_4 core and SiO_2 shell, respectively, EDS measurements were performed on the two separate sites on this two-dimensional TEM image. The results (Figure 10b and 10c) showed that the element of cobalt was found only in the core position (EDS1), not in the shell position (EDS2). Both positions showed the presence of the elements of silicon and oxygen, consistent with the presence of silica. The detection of SiO_2 in the image of the core is anticipated as the silica shell will be present above and below the cores on the third spatial dimension. Moreover, the relative amount of oxygen element in the core position was higher than that in the shell position, as expected with the Co_3O_4 cores having a higher density of atomic oxygen (1.0×10^5 mol m^{-3}) than that of SiO_2 (7.2×10^4 mol m^{-3}) assuming the density of the material is not significantly altered from that of the bulk. These observations are consistent with a composite structure of the cobalt oxide cores with silica shells. Further, the measured XRD pattern (Figure 10d) confirmed the chemical identity of the cobalt oxide cores as Co_3O_4.

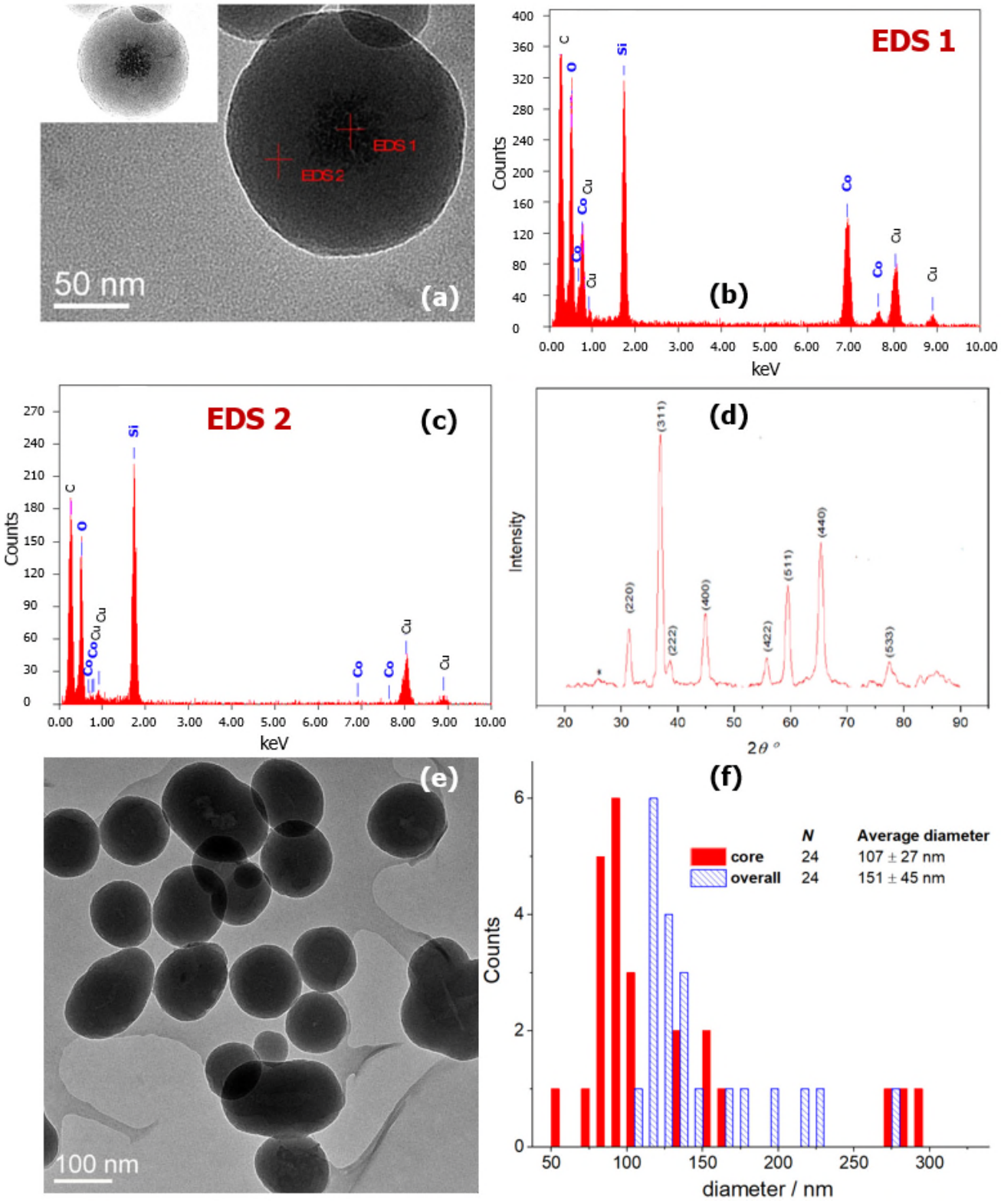

Figure 10. (a) TEM image of a single Co_3O_4@SiO_2 nanoparticle. Inlay shows the clear intensity profile of its core-shell structure after brightness and contrast adjustments. (b) 'EDS1' and (c) 'EDS2' are the EDS analysis measured at the correspondingly labelled spots in (a). (d) XRD pattern of Co_3O_4@SiO_2 NPs. (e) TEM images of more Co_3O_4@SiO_2 nanoparticles and (f) the measured diameters for both the cores and the entire particles.

2.7. Cyclic voltammetry of Co_3O_4@SiO_2 NPs

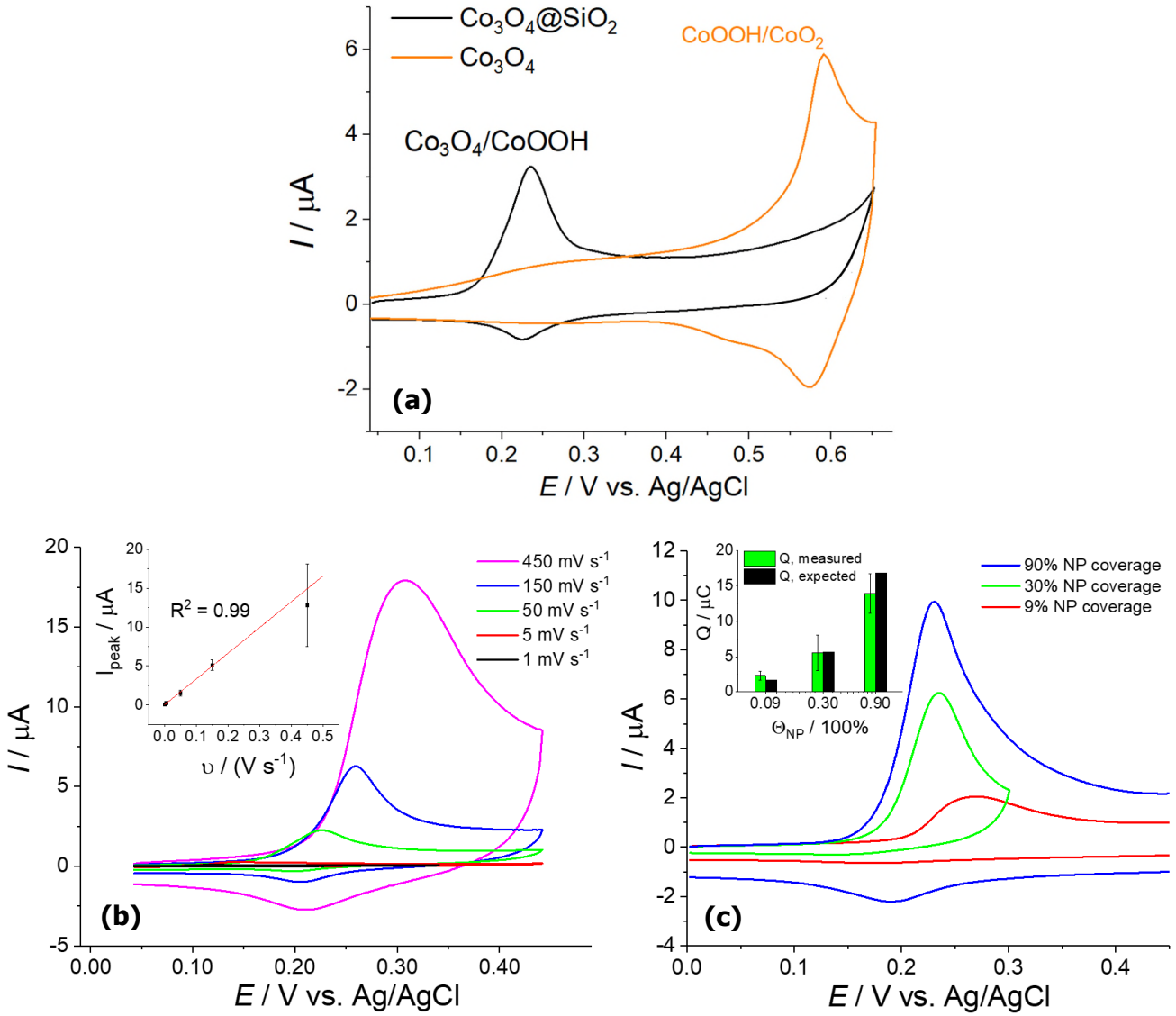

Figure 11. (a) Anodic CVs of a 3 mm-diameter GC electrode modified with Co_3O_4@SiO_2 NPs immersed in 0.1 M KCl + 20 mM KOH solutionsm, in comparison with that of the bare Co_3O_4 NPs. Scan rate 50 mV s^{-1}. (b) The CVs measured at varying scan rates of 5 to 450 mV s^{-1}. Inlay is the plot of peak current as a function of scan rate. (c) The CVs measured at varying NP surface coverages of 9% to 90% of a monolayer with a scan rate of 50 mV s^{-1}. Inlay is the plot of charge measured from the peak area as a function of NP coverage.

To check for electro-activity of the synthesised Co_3O_4@SiO_2 NPs, we performed cyclic voltammetry first from 0 V to +0.65 V. Specifically, the CV of a glassy carbon macroelectrode modified with 0.6 µg

of Co_3O_4@SiO_2 NPs, equivalent to an NP coverage of *ca.* 30% (See SI section 5a), was recorded in the same electrolyte as used above, namely 20 mM KOH + 0.1 M KCl. Surprisingly, a single oxidation peak was observed occurring at *ca.* +0.2 V (Figure 11a), a very similar potential to that of the oxidation peak of Co_3O_4 to CoOOH found in the CVs of drop-cast Co_3O_4 NPs. Further studies show that (Figure 11b) the peak current was found to be directly proportional to the scan rate, indicating the oxidation of a surface-bound species. Moreover, a small reduction peak in the backward scan was seen, with a peak-to-peak separation of 10 mV with the oxidation peak, suggesting the quasi-reversibility of the surface oxidation process. The mid-potential ($E_{1/2}$ = 0.230 V) of the peak pair was close to the thermodynamic potential (+0.22 V vs. Ag/AgCl) for the electrode couple of Co_3O_4/CoOOH. Also importantly, Figure 11c shows that the oxidative charge transferred was proportional to the nanoparticle surface coverage/loading on the carbon electrode surface; and the amounts of the charge measured were consistent with the assumption that only one monolayer of the surfaces of the Co_3O_4 cores was oxidised to CoOOH (See SI section 5b). These observations strongly confirmed that the oxidation peak at 0.2 V was due to the reaction 4. That said, the Co_3O_4 cores remained electro-active despite the present silica shells. Given that the average shell thickness is 22 nm, much bigger than the usual electron tunnelling distance (1~2 nm), the shells were considered either highly porous and/or at least some were broken.[24]

On the other hand, an unusual behaviour associated with the pH dependence of this process was discovered. Figure 12a shows that the peak potential shift with pH was found to be -80 ± 30 mV / pH, which deviated from the Nerstain slope of -59 mV / pH (298 K). This suggested a possible involvement of another chemical process. It is proposed in the literature[37] that, as shown in the Figure 12c, an alkali-metal cation intercalated structure may exist for cobalt oxyhydroxide (CoOOH). To explore whether the oxidation process was accompanied with the insertion of K^+ used in our experiements forming the intercalated structure, the CVs were also recorded in the solutions of different KCl concentrations at a fixed pH of 12.70. Consequently, Figure 12b shows that

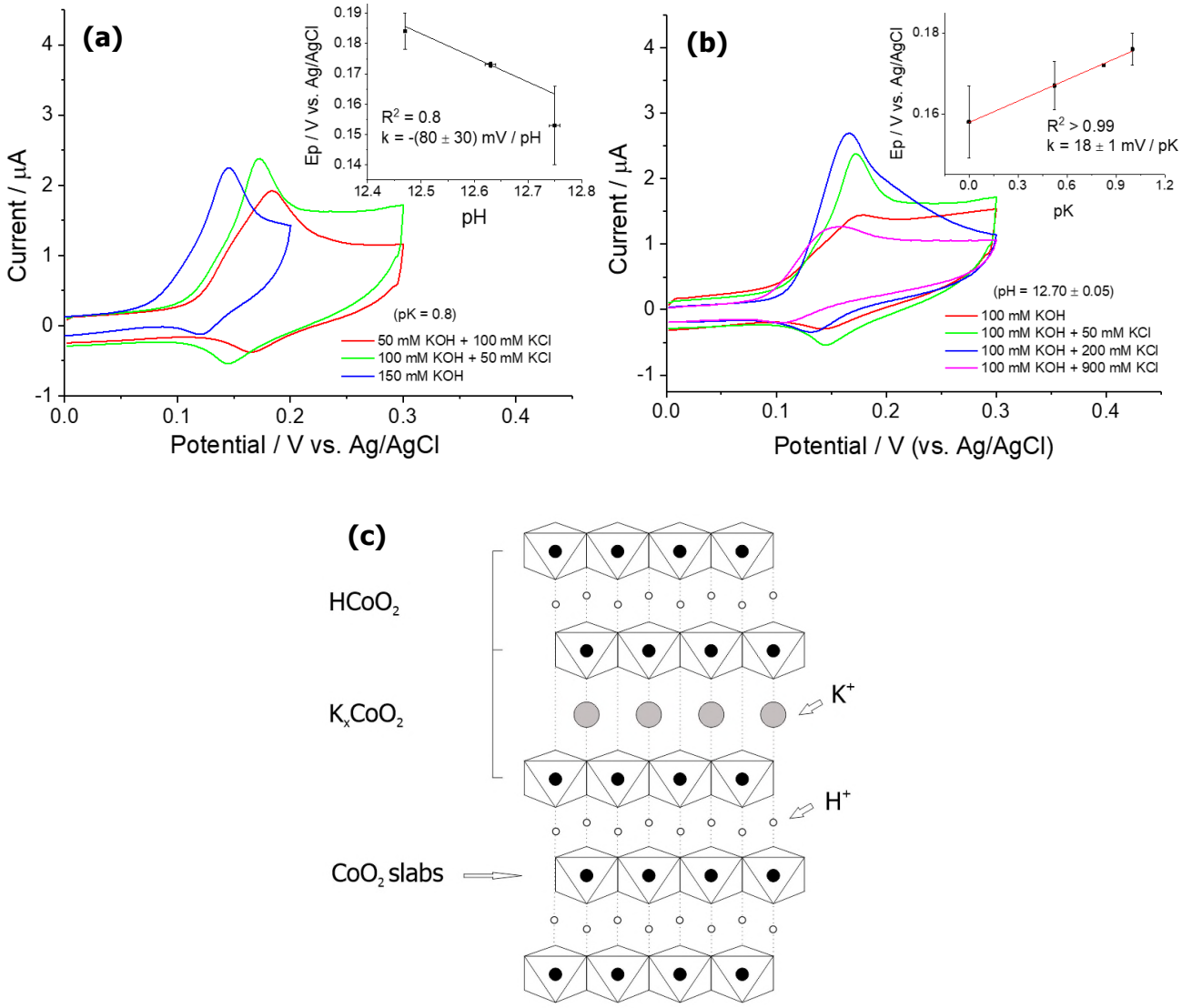

Figure 12. (a) Voltammograms of the oxidation of Co_3O_4@SiO_2 NPs using GC electrodes at varying pH from 12.30 to 12.75 with a fixed potassium cation concentration of 0.15 M. (b) Voltammograms of the oxidation of Co_3O_4@SiO_2 NPs using GC electrodes at varying pK (pK = -log[K^+]) from 0 to 1.0 with a fixed pH of 12.70 ([KOH] = 0.1 M), measured by a pH meter. (c) Schematic illustration of the suggested interstratified slab packing in the alkali-metal cation inserted cobalt oxyhydroxide structure. Adapted from Ref [37] for K^+ cations.

the peak potential indeed varied in a way the electrode reaction was favoured by a higher concentration of potassium cation at a slope of 18 ± 1 mV per pK (pK = -log[K^+]). It follows that the formation of CoOOH on the surface of the NP cores probably involves partial K^+ insertion. Therefore, the oxidation mechanism of Co_3O_4 cores was modified to:

$Co_3O_4 + (0.31\pm0.02)\ K^+ + (0.64\pm0.51)\ H_2O + (1.36\pm0.51)\ OH^- \rightarrow 3\ CoOO(H_{0.88\pm0.43}K_{0.11\pm0.1}) + e^-$ (17)

Possibly, the formation of potassium cation inserted CoOOH inhibited their further oxidation to CoO_2. Similar experiments were attempted on the CVs of drop-cast Co_3O_4 NPs but unsuccessful due to the difficulty in defining the precise peak potential of the not well-defined peaks.

2.8. Cyclic voltammetry of hydroxide ion oxidation mediated by Co_3O_4@SiO_2 NPs

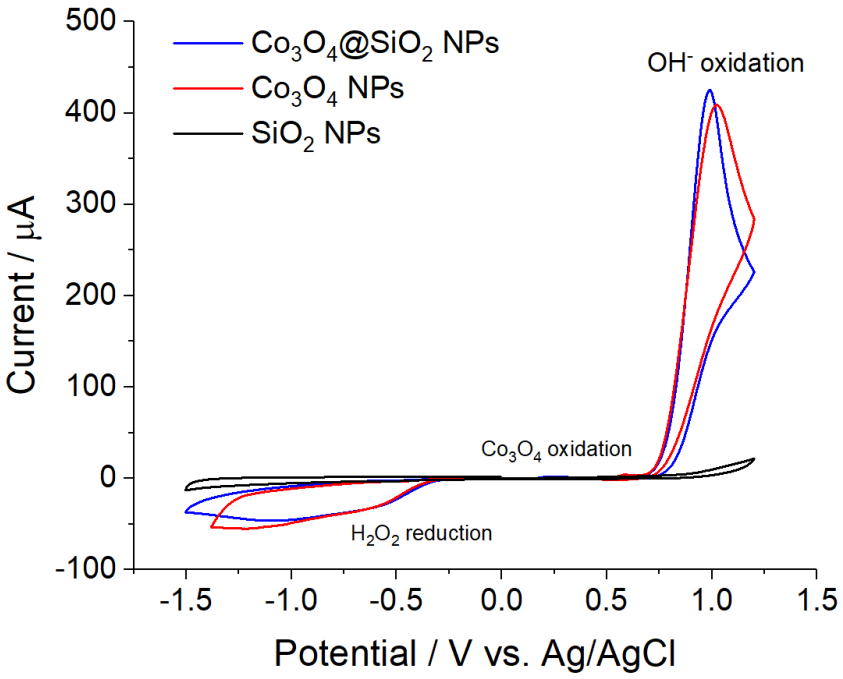

Figure 13. Overall CVs of modified GC electrodes (*d* = 3.00 mm, NP surface coverage *ca.* 30% of a monolayer) with Co_3O_4@SiO_2 NPs (blue), Co_3O_4 NPs (red) and SiO_2 NPs (black) in N_2-saturated 0.1 M KCl + 20 mM KOH solutions. Scan rate 50 mV s^{-1}.

To investigate the activity of the Co_3O_4 cores towards OH^- oxidation, the potential region of the CV was extended to a more positive potential of +1.2 V and then to the negative potential of -1.5 V. Strikingly, an almost identical oxidation wave with a peak potential of 1.0 V to the one found in the CV of bare Co_3O_4 NPs was seen. No peaks were observed in the potential region when using modified electrodes with SiO_2 NPs of a similar size (See Figure S3 in SI section 6) to those of the two types of

'cobalt' particles. These observations therefore evidenced that the cobalt oxide cores were also electro-active towards the OH^- oxidation despite the silica shell which was thus inferred to be imperfect. In the cathodic potential region of 0 to -1.5 V, a very similar reduction wave with a peak potential of -1.1 V, with a shoulder peak at -0.6 V, was seen. The peak potentials were consistent with those found in the CVs of bare Co_3O_4 NPs (See Section 2.4), therefore indicating that the product of OH^- oxidation catalysed by the Co_3O_4 cores was also very likely H_2O_2.

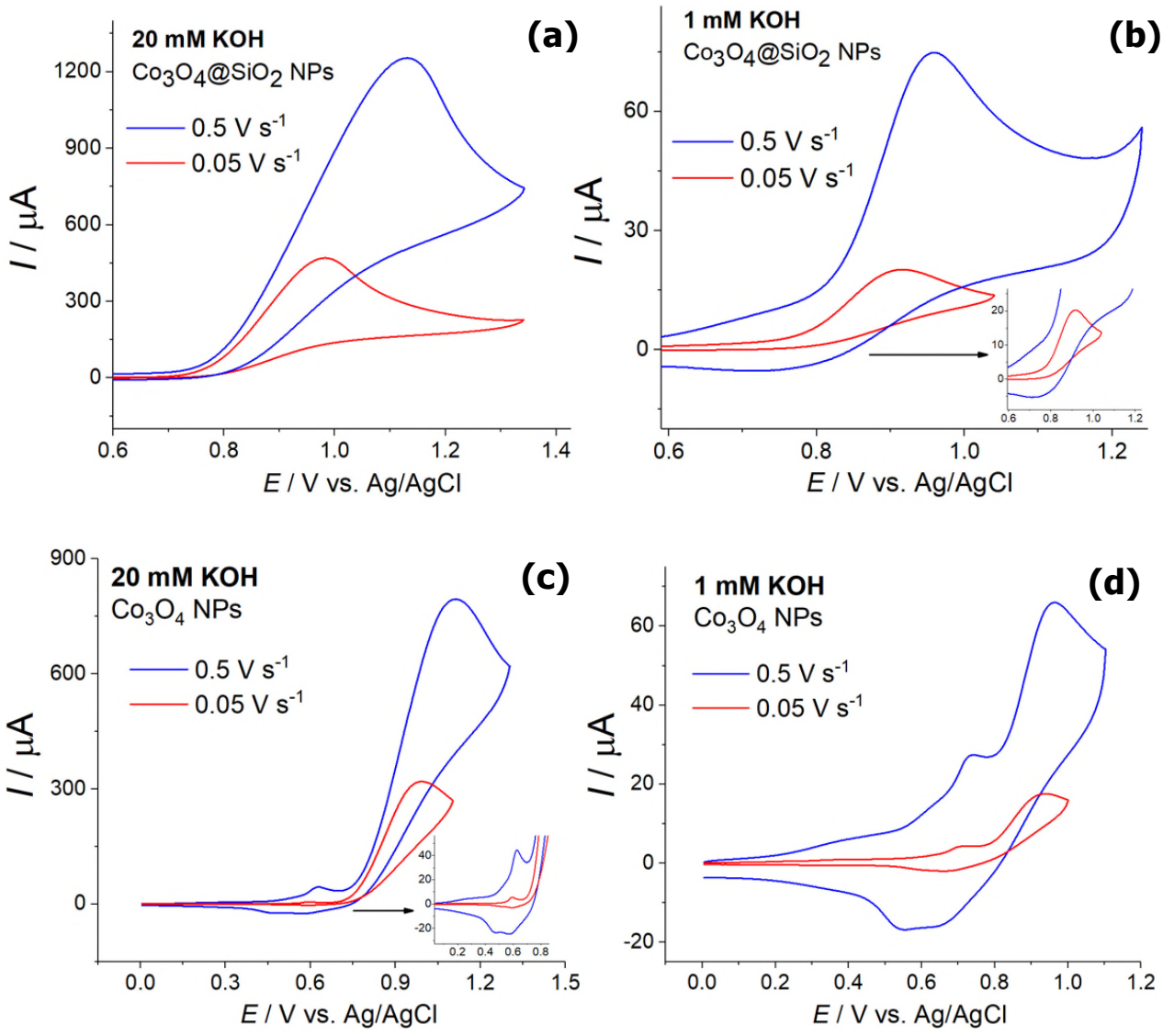

Figure 14. Anodic voltammograms of modified GC electrodes with Co_3O_4@SiO_2 NPs in 0.1 M KCl solutions containing (a) 0.1 M KCl + 20 mM KOH, (b) 0.1 M KCl + 1 mM KOH; and with bare Co_3O_4 NPs in (c) 0.1 M KCl + 20 mM KOH, (d) 0.1 M KCl + 1 mM KOH. Scan rate 0.05 and 0.5 V s^{-1}.

Considering the reaction process of the core oxidation, we discovered that the oxidation mechanism of OH^- on the Co_3O_4@SiO_2 may be slightly different from the one for the mediated reaction by bare Co_3O_4 NPs. In the KOH solutions with a concentration of 20 mM, the voltammograms at a much higher scan rate of 0.5 V s^{-1} (Figure 14a) remained similar with no more features observed. However, using a KOH solution with a much lower concentration of 1 mM and at the higher scan rates of 0.5 V s^{-1}, a reductive counterpart of the oxidation wave with a peak potential of nearly +0.75 V was observed (Figure 14b)! This was tentatively attributed to the immediate reduction of the electro-generated HO• radicals from OH^- oxidation (See below). In contrast, for the voltammograms of bare Co_3O_4 NPs (Figure 14c and 14d) under the same conditions, apart from the increase of the seemingly adsorption peak (at +0.45 V in 20 mM KOH and +0.55 V in 1 mM KOH) which was associated with NP oxidation as seen before, the back peak of the OH^- oxidation was not observed. This may suggest that the silica shell is not passive but rather may be able to stabilise the short-lived HO•, as supported by the observations on SiO_2 of this radical as an reaction intermediate in the literature.[38] Hence, the reaction mechanism of OH^- oxidation mediated by Co_3O_4@SiO_2 NP was modified to

$$OH^- \xrightarrow{Co_3O_4(s)} HO\bullet + e^- \quad (18)$$

$$HO\bullet \overset{SiO_2}{\rightleftharpoons} HO\bullet\ (ads) \quad (19)$$

$$HO\bullet\ (ads) + e^- \rightarrow OH^-\ (\text{at fast scan rates}) \quad (20)$$

$$HO\bullet\ (ads) \rightarrow \tfrac{1}{2}\ H_2O_2\ (\text{at slow scan rates}) \quad (21)$$

where the observation of the concentration dependence of the visibility of the back peak is consistent with the likely second order kinetics for HO• dimerisation.

2.9. Single particle electrochemistry of Co_3O_4@SiO_2 NPs

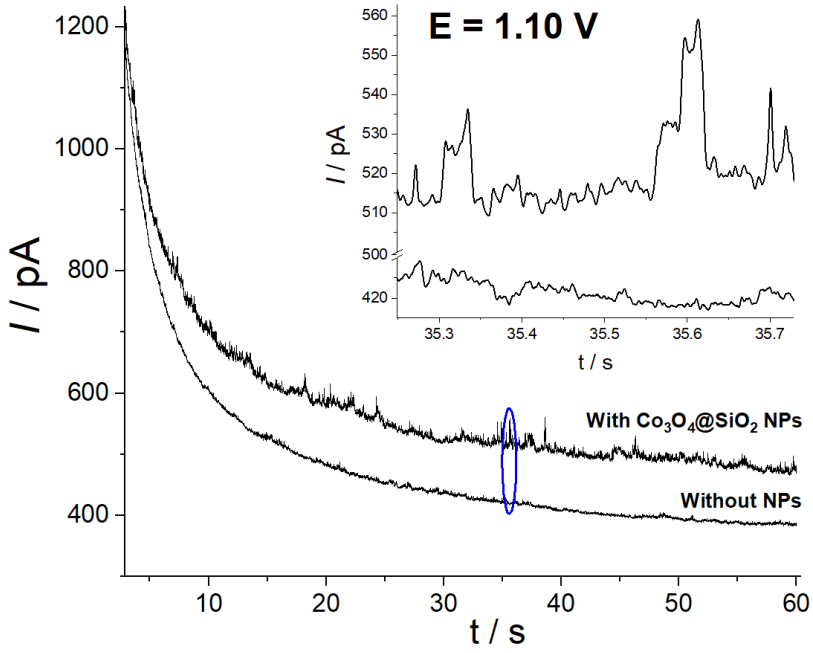

Figure 15. (a) Chronoamperograms (at 1.10 V vs. Ag/AgCl) of a clean carbon micro-disc electrode (d=7 µm) immersed in a 20 mM KOH + 0.1 M KCl solution with and without 42 pM Co_3O_4@SiO_2 NPs. Inlay shows the examples of current spikes and steps from the current-time traces highlighted by the blue circle.

Having evidenced that the silica-coated Co_3O_4 NPs catalysed the OH^- oxidation in a similar way to the bare Co_3O_4 particles, and that the impact step currents of single Co_3O_4 NPs levelled out above +1.0 V vs. Ag/AgCl, the peak potential as seen from the voltammograms of drop-cast Co_3O_4, we briefly performed the nano-impacts of the core-shell NPs at a very oxidising potential of 1.1 V to compare their *limiting* catalytic activity with that of the bare Co_3O_4 NPs at the single particle level. Experimentally, chronoamperometry of a clean carbon micro-disc electrode dipped in a solution of 20 mM KOH + 0.1 M KCl in the absence of Co_3O_4@SiO_2 NPs at a fixed potential of 1.10 V was recorded. Very few signals (in total N = 3 within 180 s) were found on the fluctuating baseline (Figure 15). In the presence of *ca.* 40 pM Co_3O_4@SiO_2 NPs, a total number of 151 current transients were detected, evidencing the impacts of the core-shell NPs with the electrode surface. The distribution of the impact durations shows a continuum with no obvious discreteness in the cumulative frequency plot, and

therefore the spike-shaped transients were considered simply as the step-shaped transients of a shorter duration (See Figure S4 in SI section 7). Moreover, these transients have much shorter durations of 39 ± 24 ms than those of the current steps for the impacts of the bare Co_3O_4 NPs (130 ± 40 ms) despite the lower diffusional mobility of the larger coated particles. This may result from the coating of insulating silica on the Co_3O_4 cores that possibly leads to a decreased quality of electrical contact formed upon the impacts between the particles and the carbon electrode surface. At the potentials more negative than +0.7 V, No impact signals were found (See Figure S5 in SI section 8). Given that the threshold potential, above which the current steps were found in the impact experiments of individual Co_3O_4 NPs, is almost that of the catalytic current in the CV of drop-cast Co_3O_4 ensembles, which is also very similar to the potential found in the CV of drop-cast Co_3O_4@SiO_2 NPs, it thus infers that those current transients were due to the catalysis of the impacting NPs towards the OH^- oxidation.

The catalytic impact responses of the core-shell NPs have an average frequency of 0.84 ± 0.16 s^{-1}, consistent with the predicted 0.70 s^{-1} assuming a steady-state diffusional flux of the NPs towards the electrode surface. This confirms the impacts of individual *single* core-shell NPs, as well as no sedimentation in their colloidal suspension, unlike the bare Co_3O_4 NPs, which is consequently attributed to the SiO_2 shells preventing particle agglomeration.[39]

Figure 16 (blue curve) depicts the current distribution of the impact transients, giving a mean impact current of 12.2 ± 3.5 pA. Since the catalysis reaction occurred at the particle-solution interface, the current measured is expected to be proportion to the electro-active surface area of the individual impacting NPs. At this time, it is reminded that from the electron microscopic measurements, the core diameter of the Co_3O_4@SiO_2 NPs was 107 ± 27 nm and the particle diameter of Co_3O_4 NPs 75 ± 22 nm, giving a surface area ratio of 2.0 ± 0.8. Then for a straight comparison on the relative sizes of

the two types of particles based on the impact currents, the current height distribution of the transient responses measured from the impact experiments of Co_3O_4 NPs is also plotted (the red curve in Figure 16), giving an average impact current of 6.4 ± 4.2 pA. As such, the current of the Co_3O_4 cores was found to be 1.9 ± 1.4 times that of the bare Co_3O_4 NPs, suggesting the same ratio of the surface area of a single Co_3O_4 core to that of a bare Co_3O_4 NP, which agrees well with that measured using electron microscopy. Summarily presented in the inlay is the strong correlation between the measured impact currents and the estimated particle surface areas of the two types of particles. These results, therefore, show at the single particle level, the preserved electro-activity of the silica-coated Co_3O_4 NPs from the bare ones and hence further supports the interference of the imperfection of the silica shells.

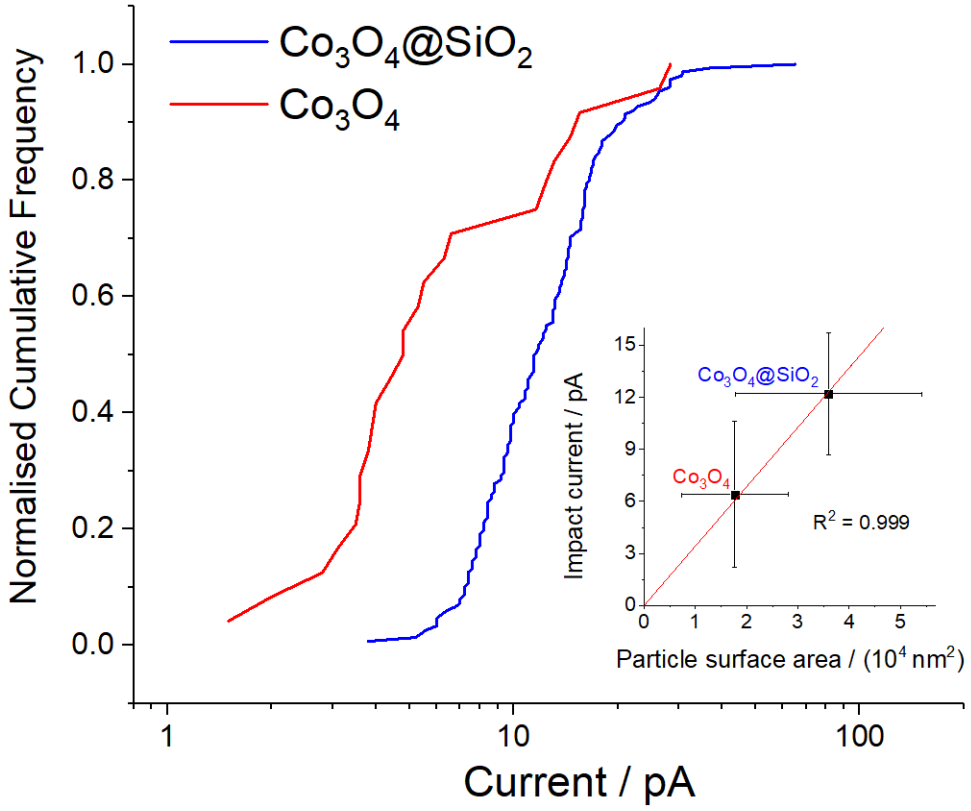

Figure 16. (a) Cumulative frequency (normalised to the total number of impact events) as a function of measured current for the impact transients measured in the impact experiments of Co_3O_4@SiO_2 NPs (blue) and Co_3O_4 NPs (red). Inlay is the correlation chart between the impact current and the Co_3O_4 surface area of individual particles. Note that the standard deviation bars reflect more the width of the current/surface area distribution than the measurement errors. The linear fitting shows a coefficient of determination (R^2) as 0.999.

3. Conclusions

Co_3O_4 nanoparticles have been shown to be an effective electro-catalyst for hydroxide ion oxidation with *hydrogen peroxide* rather than dioxygen as the predominant initial oxidation product of the electron transder. Single particle electrochemistry further indicated that the rate of this catalysis is limited by the rate of the surface catalytic process. Further, silica-coated Co_3O_4 nanoparticles were synthesised and their structures were characterised *via* a combination of TEM, EDS and XRD techniques. Similar electrochemistry results to those of bare Co_3O_4 nanoparticles were obtained and our studies demonstrated generally unchanged electro-catalytic activity towards OH^- oxidation, therefore suggesting the imperfect coating of the Co_3O_4@SiO_2 NPs. Last, but not least, the UV spectroscopy shows the catalytic activity of Co_3O_4 NPs towards the chemical decomposition of H_2O_2. As studies have also shown their electro-catalytic activity towards oxygen reduction reaction, this may in turn offer a mechanistic pathway for a 4-electron reduction to water *via* hydrogen peroxide as an initial reaction intermediate, with Co_3O_4 NPs thus acting as bifunctional electrochemical and chemical catalysts, as shown for Fe_2O_3 NPs.[14]

4. Experimental

4.1. Chemicals

Cobalt (II) dicobalt (III) oxide (Co_3O_4) nanoparticles (NPs), potassium hydroxide solutions (0.974 M, purity ≥ 99.0%), calcium hydroxide (95%), hydrogen peroxide (30 wt% in H_2O), potassium chloride (≥ 99.0%), cobalt (II) nitrate hexahydrate ($Co(NO_3)_2{\cdot}6H_2O$, 99.999%), tetraethyl orthosilicate (98%), N,N-Dimethyl formamide (99.8%) and polyvinylpyrrolidone (molecular weight 40000) were purchased from Sigma-Aldrich, UK and used as received. Nitrogen and oxygen gas cylinders was supplied from

British Oxygen Company, Surrey, U.K. All solutions were prepared with de-ionised water of resistivity of 18.2 MΩ cm at 298 K (Millipore).

4.2. Synthesis of Co_3O_4@SiO_2 NPs

Prior to the synthesis of the core-shell Co_3O_4@SiO_2 NPs, Co_3O_4 nanoparticles were first synthesized by thermal decomposition of cobalt (II) nitrate hexahydrate ($Co(NO_3)_2 \cdot 6H_2O$) as described in a previous study by Volokhova.[40] Specifically, 0.62 g of $Co(NO_3)_2 \cdot 6H_2O$ was dissolved in 10 mL of anhydrous dimethylformamide and then 0.3 g of polyvinylpyrrolidone was added to the solution, which was stirred for 30 min. The reaction mixture was thermostated at 180°C for four days. The initially transparent purpel solution turned black-brown. Then 50 mL of ethanol was added to the final black-brown colloid solution and washed twice to remove excess surfactant and reaction byproducts. The precipitate of nanoparticles was collected by centrifugation and kept in ethanol solution.

Second, coating of the obtained Co_3O_4 nanoparticles with SiO_2 was carried out according to the similar procedure as previously described.[40, 41] Prior to the synthesis, 100 mL of ethanol and 10 mL of deionised water were stirred at 200 rpm for 10 min. 25 mg of nanoparticles were dissolved in ethanol (2 ml) and added to the mixture of water and ethanol and stirred for 30 min. After that, 25 mL of NH_4OH (28%) were added dropwise to the solution and stirred for 30 min. Meanwhile, tetraethyl orthosilicate (TEOS) solution was made. 1 ml of TEOS was dissolved in 30 ml ethanol and stirred for 30 min. Then 4 ml of TEOS/ethanol mixture was added dropwise for 8 h into the nanoparticle solution. The precipitate was collected by centrifugation and washed twice to remove excess surfactant and reaction byproducts. Collected nanoparticles were stored in ethanol solution.

4.3. Synthesis of SiO_2 NPs

The silica nanoparticles were prepared with a modified procedure of a previous study.[42] 6.9 ml of TEOS was hydrolysed in 250 ml of ethanol with continuous stirring with a speed of 230 rpm. After 30 min, a mixture of deionised water (25 ml) and ammonium hydroxide solution (2.5 ml) were added into the reaction solution and kept stirring for 4 hours until the mixture turned into a milky solution. Then, reaction mixture were washed with ethanol twice and dried with rotary evaporator for 1 hour.

4.4. Material Characterisation

The scanning electron microscopy (SEM) images of Co_3O_4 NPs were obtained using a Zeiss Sigma 300 FEG-SEM with an accelerating voltage of 2.0 kV. Prior to the measurements, the NPs were suspended in water and drop-casted onto a cleaned glassy carbon stub, which was subsequently dried overnight in vacuum. Energy Diperseive Spectroscopy (EDS) were also performed on those NPs.

Transmission Elecron Microscopy (TEM) images of Co_3O_4@SiO_2 and SiO_2 NPs were obtained using JEOL JEM 2200FS and JEOL JEM 1400EX electron microscope, respectively. Diluted samples for TEM measurements were prepared by drop-cast the pre-suspended NPs on a copper grid and dried overnight in vacuum. EDS were also performed on the specific sites of Co_3O_4@SiO_2 NPs to study the elemental content of core and shell.

Powder X-ray Diffraction (XRD, Panalytica Xpert3) measurements of Co_3O_4@SiO_2 NPs were carried out with Cu Kα radiation (λ = 0.154 nm) with 45 kV beam voltage and 40 mA beam current. Patterns were collected in a range from 20° to 90° with the steps of 0.02° and the exposure time of 100 sec.

4.5. Cyclic voltammetry of hydroxide ion oxidation on a glassy carbon electrode modified with Co_3O_4 and Co_3O_4@SiO_2 NPs

A suspension of Co_3O_4 NPs or Co_3O_4@SiO_2 NPs (0.1 mg mL^{-1}) was prepared by adding 0.5 mg of the particles to 5 mL of water. The particle suspension was vortexed for 10 seconds followed by 30 seconds' resting; this was repeated six times. A glassy carbon (GC) electrode (*d* = 3.00 mm) was polished with 0.3 and 0.05 µm-sized alumina particles on microcloths in sequence. The as-prepared suspension was then drop-cast on the GC electrode and dried under an N_2 flow.

Cyclic voltammetry was conducted in 0.1 M KCl solutions containing 20 mM KOH, using a three-electrode system under potential control *via* a µAutolab TypeII potentiostat (Metrohm-Autolab BV, The Netherlands) thermostated at 298 K. The modified GC electrode was used as the working electrode, a platinum foil as the counter electrode and a silver/silver chloride electrode (3.4 M KCl, +0.205 V vs. SHE at 298 K) as the reference electrode. For the experiments using oxygen-saturated solutions, pure oxygen gas was bubbled through the solutions for *ca.* 10 mins to reach a steady, saturated condition of the dissolved gas.

4.6. Kinetic study of hydrogen peroxide decomposition using UV-vis spectroscopy

The kinetics of hydrogen peroxide decomposition in 20 mM KOH was studied using UV-vis measurements (λ = 240-300 nm) with a Shimadzu UV-1800 spectrophotometer, using quartz cuvettes (Quartz SUPRASIL, Hellma Analytics) with an optical light path of 10 mm.

4.7. Nano-impact experiments of Co_3O_4 and Co_3O_4@SiO_2 NPs

An aqueous suspension of either Co_3O_4 NPs (10 mg mL^{-1}) or Co_3O_4@SiO_2 NPs (0.03 mg mL^{-1}) was prepared. Dispersed suspensions were obtained by vortexing as described above. Nano-impact experiments were carried out using a low-noise homemade potentiostat at 298 K which has been described previously.[43] Prior to the measurements, potassium hydroxide and chloride were added to the particle suspensions to give a final concentration of 20 mM KOH + 0.1 M KCl. A clean carbon micro-disc electrode (ALS Co., Ltd, d = 7.0 μm) was inserted to the mixture. In these fresh particle suspensions (ageing time < 15 mins) current-time measurements (or chronamperometry) were made at varying fixed potentials. Counting and analysis of the impact signals were performed in Origin 2017 Pro.

Conflicts of interest

The authors declare no conflict of interest.

Acknowledgements

M.V. A.B. and L.S. acknowledge financial funding from the Estonian Research Council (Personal Grant PUT 1046) and the European Regional Development Fund (project no. TK 134). M.T. thanks Archimedes for the Kristjan Jaak Scholarship. M.Y. acknowledges funding via the EPSRC Industrial CASE award (EP/N509711/1).

Keywords: cobalt (II) dicobalt (III) oxide nanoparticles; core-shell nanoparticles; electrocatalysis; hydroxide ion oxidation; nano-impacts

References

[1] T. Zhang, C. He, F. Sun, Y. Ding, M. Wang, L. Peng, J. Wang, Y. Lin, *Scientific Reports* **2017**, *7*, 43638.

[2] H. Ha, K. Jin, S. Park, K.-G. Lee, K. H. Cho, H. Seo, H.-Y. Ahn, Y. H. Lee, K. T. Nam, *The Journal of Physical Chemistry Letters* **2019**, *10*, 1226-1233.

[3] G. Rajeshkhanna, G. R. Rao, *International Journal of Hydrogen Energy* **2018**, *43*, 4706-4715.

[4] E. Zhang, Y. Xie, S. Ci, J. Jia, Z. Wen, *Biosensors and Bioelectronics* **2016**, *81*, 46-53.

[5] a) Y. Liang, Y. Li, H. Wang, J. Zhou, J. Wang, T. Regier, H. Dai, *Nature Materials* **2011**, *10*, 780; b) L. Xu, Q. Jiang, Z. Xiao, X. Li, J. Huo, S. Wang, L. Dai, *Angewandte Chemie International Edition* **2016**, *55*, 5277-5281.

[6] M. Hamdani, R. Singh, P. Chartier, *International Journal of Electrochemical Science* **2010**, *5*, 556-577.

[7] I.-H. Yeo, PhD thesis, Iowa State University (US), 1987.

[8] C. C. McCrory, S. Jung, J. C. Peters, T. F. Jaramillo, *Journal of the American Chemical Society* **2013**, *135*, 16977-16987.

[9] B. Su, Z.-C. Cao, Z.-J. Shi, *Accounts of Chemical Research* **2015**, *48*, 886-896.

[10] a) B. S. Yeo, A. T. Bell, *Journal of the American Chemical Society* **2011**, *133*, 5587-5593; b) Z. Zhuang, W. Sheng, Y. Yan, *Advanced Materials* **2014**, *26*, 3950-3955; c) S. Liu, L. Li, H. S. Ahn, A. Manthiram, *Journal of Materials Chemistry A* **2015**, *3*, 11615-11623; d) J. Wu, Y. Xue, X. Yan, W. Yan, Q. Cheng, Y. Xie, *Nano Research* **2012**, *5*, 521-530; e) Y.-R. Liu, G.-Q. Han, X. Li, B. Dong, X. Shang, W.-H. Hu, Y.-M. Chai, Y.-Q. Liu, C.-G. Liu, *International Journal of Hydrogen Energy* **2016**, *41*, 12976-12982; f) J. D. Blakemore, H. B. Gray, J. R. Winkler, A. M. Müller, *ACS Catalysis* **2013**, *3*, 2497-2500; g) J. A. Koza, Z. He, A. S. Miller, J. A. Switzer, *Chemistry of Materials* **2012**, *24*, 3567-3573.

[11] A. J. Esswein, M. J. McMurdo, P. N. Ross, A. T. Bell, T. D. Tilley, *The Journal of Physical Chemistry C* **2009**, *113*, 15068-15072.

[12] N. H. Chou, P. N. Ross, A. T. Bell, T. D. Tilley, *ChemSusChem* **2011**, *4*, 1566-1569.

[13] a) S. Chen, Y. Zhao, B. Sun, Z. Ao, X. Xie, Y. Wei, G. Wang, *ACS Applied Materials & Interfaces* **2015**, *7*, 3306-3313; b) T. Watanabe, Y. Einaga, *Analytical chemistry* **2017**, *89*, 7139-7144.

[14] K. Shimizu, L. Sepunaru, R. G. Compton, *Chemical Science* **2016**, *7*, 3364-3369.

[15] C. C. Neumann, E. Laborda, K. Tschulik, K. R. Ward, R. G. Compton, *Nano Research* **2013**, *6*, 511-524.

[16] H. S. Toh, C. Batchelor-McAuley, K. Tschulik, M. Uhlemann, A. Crossley, R. G. Compton, *Nanoscale* **2013**, *5*, 4884-4893.

[17] S. J. Cloake, H. S. Toh, P. T. Lee, C. Salter, C. Johnston, R. G. Compton, *ChemistryOpen* **2015**, *4*, 22-26.

[18] X. Li, H. Hodson, C. Batchelor-McAuley, L. Shao, R. G. Compton, *ACS Catalysis* **2016**, *6*, 7118-7124.

[19] X. Jiao, C. Batchelor-McAuley, C. Lin, E. Kätelhön, E. E. Tanner, N. P. Young, R. G. Compton, *ACS Catalysis* **2018**, *8*, 6192-6202.

[20] a) X. Li, C. Batchelor-McAuley, S. A. Whitby, K. Tschulik, L. Shao, R. G. Compton, *Angewandte Chemie International Edition* **2016**, *55*, 4296-4299; b) X. Li, C. Lin, C. Batchelor-McAuley, E. Laborda, L. Shao, R. G. Compton, *The Journal of Physical Chemistry Letters* **2016**, *7*, 1554-1558.

[21] C. Lin, R. G. Compton, *The Journal of Physical Chemistry C* **2017**, *121*, 2521-2528.

[22] a) A. N. Sekretaryova, M. Y. Vagin, A. P. Turner, M. Eriksson, *Journal of the American Chemical Society* **2016**, *138*, 2504-2507; b) L. Han, W. Wang, J. Nsabimana, J.-W. Yan, B. Ren, D. Zhan, *Faraday Discussions* **2016**, *193*, 133-139; c) E. Kätelhön, L. Sepunaru, A. A. Karyakin, R. G. Compton, *Acs Catalysis* **2016**, *6*, 8313-8320.

[23] a) T. Albrecht, S. Horswell, L. Allerston, N. Rees, P. Rodriguez, *Current Opinion in Electrochemistry* **2018**, *7*, 138-145; b) N. V. Rees, *Electrochemistry Communications* **2014**, *43*, 83-86; c) S. V. Sokolov, S. Eloul, E. Kätelhön, C. Batchelor-McAuley, R. G. Compton,

Physical Chemistry Chemical Physics **2017**, *19*, 28-43; dK. J. Stevenson, K. Tschulik, *Current Opinion in Electrochemistry* **2017**, *6*, 38-45.

[24] K. Tschulik, K. Ngamchuea, C. Ziegler, M. G. Beier, C. Damm, A. Eychmueller, R. G. Compton, *Advanced Functional Materials* **2015**, *25*, 5149-5158.

[25] L. R. Holt, B. J. Plowman, N. P. Young, K. Tschulik, R. G. Compton, *Angewandte Chemie International Edition* **2016**, *55*, 397-400.

[26] A. Earnshaw, N. N. Greenwood, *Chemistry of the Elements, Vol. 60*, Butterworth-Heinemann Oxford, **1997**.

[27] a) J. Chivot, L. Mendoza, C. Mansour, T. Pauporté, M. Cassir, *Corrosion Science* **2008**, *50*, 62-69; b) M. Bajdich, M. García-Mota, A. Vojvodic, J. K. Nørskov, A. T. Bell, *Journal of the American chemical Society* **2013**, *135*, 13521-13530.

[28] D. Li, C. Lin, C. Batchelor-McAuley, L. Chen, R. G. Compton, *Journal of Electroanalytical Chemistry* **2018**, *826*, 117-124.

[29] a) S. Daniele, M. A. Baldo, C. Bragato, G. Denuault, M. E. Abdelsalam, *Analytical Chemistry* **1999**, *71*, 811-818; b) S. H. Lee, J. C. Rasaiah, *The Journal of Chemical Physics* **2013**, *139*, 124507.

[30] Z. M. Galbács, L. J. Csányi, *Journal of the Chemical Society, Dalton Transactions* **1983**, 2353-2357.

[31] S. Sharifi, H. Shakur, A. Mirzaei, M. Hosseini, *International Journal of Nanoscience and Nanotechnology* **2013**, *9*, 51-58.

[32] R. C. Taylor, P. C. Cross, *Journal of the American Chemical Society* **1949**, *71*, 2266-2268.

[33] Y.-S. Shen, C.-C. Lin, *Water Environment Research* **2003**, *75*, 54-60.

[34] J. Rabani, S. O. Nielsen, *The Journal of Physical Chemistry* **1969**, *73*, 3736-3744.

[35] A. Einstein, *Annalen der Physik* **1905**, *322*, 891-921.

[36] R. Compton, C. Banks, *Undestanding Voltammetry*, **2018**, p. 172.

[37] M. Butel, L. Gautier, C. Delmas, *Solid State Ionics* **1999**, *122*, 271-284.

[38] a) E. Giamello, B. Fubini, M. Volante, D. Costa, *Colloids and Surfaces* **1990**, *45*, 155-165; b) Y. Gong, D. P. Wang, R. Wu, S. Gazi, H. S. Soo, T. Sritharan, Z. Chen, *Dalton Transactions* **2017**, *46*, 4994-5002.

[39] H. D. Ackler, R. H. French, Y.-M. Chiang, *Journal of Colloid and Interface Science* **1996**, *179*, 460-469.

[40] Maria Volokhova, Aleksei Boldin, Joosep Link, Masahiko Tujimoto, Raivo Stern , Liis Seinberg. Submitted to Chem. Comm. in January 2020.

[41] K. Kohara, S. Yamamoto, L. Seinberg, T. Murakami, M. Tsujimoto, T. Ogawa, H. Kurata, H. Kageyama, M. Takano, *Chemical Communications* **2013**, *49*, 2563-2565.

[42] D. Green, J. Lin, Y.-F. Lam, M.-C. Hu, D. W. Schaefer, M. Harris, *Journal of Colloid and Interface Science* **2003**, *266*, 346-358.

[43] C. Batchelor-McAuley, J. Ellison, K. Tschulik, P. L. Hurst, R. Boldt, R. G. Compton, *Analyst* **2015**, *140*, 5048-5054.